



Current Perspectives

Comparison of the ferromagnetic Blume–Emery–Griffiths model and the AF spin-1 longitudinal Ising model at low temperature

M.T. Thomaz^{a,*}, E.V. Corrêa Silva^b^a Instituto de Física, Universidade Federal Fluminense, Av. Gal. Milton Tavares de Souza s/no, CEP 24210-346, Niterói, RJ, Brazil^b Departamento de Matemática, Física e Computação, Faculdade de Tecnologia, Universidade do Estado do Rio de Janeiro, Rodovia Presidente Dutra km 298 s/no, Pólo Industrial, CEP 27537-000, Resende, RJ, Brazil

ARTICLE INFO

Article history:

Received 14 September 2015

Accepted 18 October 2015

Available online 21 October 2015

Keywords:

Quantum statistical mechanics

Blume–Emery–Griffiths model

BEG model

Ising model

Spin-1

Staggered

Thermodynamics

Optical device

ABSTRACT

We derive the exact Helmholtz free energy (HFE) of the standard and staggered one-dimensional Blume–Emery–Griffiths (BEG) model in the presence of an external longitudinal magnetic field. We discuss in detail the thermodynamic behavior of the ferromagnetic version of the model, which exhibits magnetic field-dependent plateaux in the z-component of its magnetization at low temperatures. We also study the behavior of its specific heat and entropy, both per site, at finite temperature. The degeneracy of the ground state, at $T=0$, along the lines that separate distinct phases in the phase diagram of the ferromagnetic BEG model is calculated, extending the study of the phase diagram of the spin-1 anti-ferromagnetic (AF) Ising model in S.M. de Souza and M.T. Thomaz, J. Magn. and Magn. Mater. 354 (2014) 205 [5]. We explore the implications of the equality of phase diagrams, at $T=0$, of the ferromagnetic BEG model with $\frac{K}{J_1} = -2$ and of the spin-1 AF Ising model for $\frac{D}{J_1} > \frac{1}{2}$.

© 2015 Published by Elsevier B.V.

1. Introduction

For a long time simple 1-D spin models have been used as toy models for a better understanding of real systems with coupled spins. Experimental verification of the results derived from those toy spin models is difficult, given the complexity of real spin systems for any spatial dimension. The development of optical devices permitted the simulation of a few 1-D spin models in arrays of cold atoms. In 2011 Simon et al. [1] simulated the 1-D spin-1/2 Ising model in the presence of a magnetic field with longitudinal and transverse components at low temperature. Such possibility encourage us to explore the thermodynamic characteristics of 1-D models.

Recently one of the authors applied the transfer matrix method [2–4] to the calculation of the exact thermodynamics of the 1-D spin-1 Ising model, with single-ion anisotropy term, in the presence of an external longitudinal magnetic field [5]. The present work extends that discussion to the classical 1-D Blume–Emery–Griffiths (BEG) model [6] with external longitudinal magnetic field. This model is classical and its exact thermodynamics can also be derived by the transfer matrix method. The presence of an extra term with respect to the 1-D Ising model with single-ion

anisotropy term can modify the behavior of the quantum chain, mainly its phase diagram at $T=0$. In the present paper we study the thermodynamics of the one-dimensional BEG model in the presence of an external longitudinal magnetic field. The phase diagram of the model is discussed in detail for the ferromagnetic case, and for two different regions of the parameter $\frac{K}{J_1}$, and complemented by the discussion on the phase diagram of the spin-1 AF Ising model [5].

In Section 2 we present the Hamiltonian of the standard BEG model in the presence of an external longitudinal magnetic field. We show the relation between the Hamiltonians of the standard and staggered versions of this model, to be used in relating their thermodynamics. In Section 3 we discuss the phase diagram, at $T=0$, of the ferromagnetic BEG model. Its thermodynamics is presented in Section 3.1 through the behavior of three thermodynamic functions per site: the z-component of the magnetization, the specific heat and the entropy. The entropy per site along each line that separates distinct phases in the diagram of the ferromagnetic BEG model is calculated at $T=0$. In Section 4 we compare the three previous thermodynamic functions of the ferromagnetic BEG model with $\frac{K}{J_1} = -2$ and the spin-1 AF Ising model at very low temperature. We also extend the discussion on the phase diagram of the spin-1 AF model in Ref. [5] in order to include the degeneracy of the ground state of the model at $T=0$. Our conclusions are presented in Section 5. In Appendix A we present the

* Corresponding author.

E-mail address: mtt@if.uff.br (M.T. Thomaz).

main steps to calculate the exact Helmholtz free energy (HFE) of the standard and staggered one-dimensional BEG model for arbitrary values of the parameters. The states and energies of the dimers present in the spin configurations of the chain are shown in Appendix B. In Appendix C we have the ground states of the BEG model in the presence of an external longitudinal magnetic field and their respective energies. Finally in Appendix D we show how to calculate the degeneracy of the ground state along the lines that separate the different phases along the diagrams of the chain models at $T=0$.

2. The Hamiltonian and HFE of the 1-D Blume–Emery–Griffiths model with a longitudinal magnetic field

Eq. (5) of Ref. [5],

$$\mathbf{H}_I^{S=1}(J, h, D) = \sum_{i=1}^N \left[JS_i^z S_{i+1}^z - hS_i^z - hS_{i+1}^z + D(S_i^z)^2 + D(S_{i+1}^z)^2 \right], \quad (1)$$

is the Hamiltonian of the one-dimensional classical spin-1 Ising model with the single-ion anisotropy term with the crystal field D , the Blume–Capel model [7,8], in the presence of an external longitudinal (z -axis) magnetic field h , symmetrized in the nearest neighbours. Here, S_i^z is the z -component of the spin-1 operator in the i -th site ($|S_i^z|^2 = 2$), and J is the exchange strength. For $J > 0$ we have the anti-ferromagnetic (AF) version of the model, whereas for $J < 0$ ferromagnetic version is obtained. We assume that $h \geq 0$, that D may have any real value, and that the chain has N sites and it is periodic, i.e. $S_{N+1}^z = S_1^z$. In this paper we use natural units $e = m = \hbar = 1$.

Adding the term $-K(S_i^z)^2(S_{i+1}^z)^2$ to Hamiltonian (1), with $K \in \mathbb{R}$, yields the Hamiltonian of the Blume–Emery–Griffiths (BEG) model [6,9]

$$\begin{aligned} \mathbf{H}_{BEG}(J, h, D, K) \\ = \sum_{i=1}^N [JS_i^z S_{i+1}^z - hS_i^z - hS_{i+1}^z + D(S_i^z)^2 + D(S_{i+1}^z)^2 \\ - K(S_i^z)^2(S_{i+1}^z)^2]. \end{aligned} \quad (2)$$

This Hamiltonian also satisfies the periodic condition. (The Hamiltonian (1) with $L=0$ in Ref. [6] describes the BEG model in a non-symmetrized form.)

Ref. [5] discusses at length which quantum state(s) is (are) favored by each term on the r.h.s. of Hamiltonian (1), regarding the minimization of energy; we will not repeat this discussion here. Let s_i^z be the eigenvalue of the operator S_i^z . In (2), the term in K will, for $K > 0$, favor the dimer states (i.e., relative to two neighboring spins) in which $s_i^z = \pm 1$, independently of their relative orientation (they may be either parallel or anti-parallel). On the other hand, for $K < 0$, the favored dimer states will be those with at least one null eigenvalue, i.e., $s_i^z = 0$. Section 3 will describe how the term in K changes the $T=0$ phase diagrams of the classical ferromagnetic spin-1 Ising models presented in Ref. [5].

The staggered BEG model in its symmetrized version reads

$$\begin{aligned} \mathbf{H}_{BEG}^{stag}(J_s, h_s, D_s, K_s) \\ = \sum_{i=1}^N \left[J_s S_i^z S_{i+1}^z - (-1)^i h_s S_i^z - (-1)^{i+1} h_s S_{i+1}^z + D_s (S_i^z)^2 \right. \\ \left. + D_s (S_{i+1}^z)^2 - K_s (S_i^z)^2 (S_{i+1}^z)^2 \right]. \end{aligned} \quad (3)$$

This Hamiltonian will also be subject to the spatial periodic condition. We assume that the chain has an even number of sites,

so $N = 2M$, in which $M \in \mathbb{N}$.

The mapping $S_i^z \rightarrow (-1)^i S_i^z$ in Hamiltonian (3) yields the relation between the standard and staggered BEG models

$$\mathbf{H}_{BEG}^{stag}(J_s, h_s, D_s, K_s) = \mathbf{H}_{BEG}(-J, h, D, K); \quad (4)$$

hence they have the same thermodynamics if $J_s = -J$, $h_s = h$, $D_s = D$ and $K_s = K$. The ferromagnetic staggered BEG model ($J_s < 0$) has the same thermodynamics as the AF standard BEG model ($J > 0$). The AF staggered BEG model ($J_s > 0$) has the same behavior as the ferromagnetic standard BEG model ($J < 0$) at any finite temperature.

From now on we will restrict our discussion to the thermodynamics of the standard Hamiltonian (2) of the BEG model. The thermodynamic behavior of the staggered BEG models at finite temperature can be obtained from the corresponding standard models by using (4).

In Appendix A we show the calculation of the exact expression of the Helmholtz free energy (HFE) of the ferromagnetic and AF BEG models in the presence of a longitudinal magnetic field by the transfer matrix method [2–4], valid at any finite temperature $T > 0$. In 1975 Krinsky and Furman [10] calculated this thermodynamic function for those BEG models. Our expression of the HFE for non-null external longitudinal magnetic field $h \neq 0$ written differently from that of Ref. [10]; ours has contributions only from real functions of the parameters of Hamiltonian (2) and of $\beta = \frac{1}{kT}$, in which k is Boltzmann's constant and T is the absolute temperature in kelvin. Although the results derived in that appendix are valid for both the ferromagnetic and the AF BEG models, in the following sections of this paper the discussion is restricted to the ferromagnetic case.

3. The phase diagram of the ferromagnetic BEG model at $T=0$

The Hamiltonian (2) can be written as the sum of Hamiltonians of dimers on neighboring sites i and $i+1$, $i \in \{1, 2, \dots, N\}$. For the dimer composed of the $(i, i+1)$ sites, we have

$$\begin{aligned} \mathbf{H}_{i,i+1}^{(D)}(J, h, D, K) \\ = JS_i^z S_{i+1}^z - hS_i^z - hS_{i+1}^z + D(S_i^z)^2 + D(S_{i+1}^z)^2 - K(S_i^z)^2(S_{i+1}^z)^2. \end{aligned} \quad (5)$$

The ferromagnetic case corresponds to $J < 0$.

Let $|s_i^z\rangle_i$ and s_i^z be the eigenstate and eigenvalue, respectively, of the z -component of the spin operator at i -th site, S_i^z , so that $S_i^z |s_i^z\rangle_i = s_i^z |s_i^z\rangle_i$, with $s_i^z \in \{-1, 0, 1\}$. The energy $\varepsilon_{i,i+1}$ of the dimer $(i, i+1)$, described by the state $|D\rangle_{i,i+1} = |s_i^z\rangle_i \otimes |s_{i+1}^z\rangle_{i+1}$ is, in units of $|J|$,

$$\begin{aligned} \frac{\varepsilon_{i,i+1}}{|J|} &= \frac{i,i+1 \langle D | \mathbf{H}_{i,i+1}^{(D)} | D \rangle_{i,i+1}}{|J|} \\ &= s_i^z s_{i+1}^z - \frac{h}{|J|} (s_i^z + s_{i+1}^z) + \frac{D}{|J|} [(s_i^z)^2 + (s_{i+1}^z)^2] \\ &\quad - \frac{K}{|J|} (s_i^z)^2 (s_{i+1}^z)^2, \end{aligned} \quad (6)$$

with $s_i^z, s_{i+1}^z \in \{0, \pm 1\}$, and $i \in \{1, 2, \dots, N\}$. All the parameters of the Hamiltonian (2) are scaled in units of $|J|$: $\frac{h}{|J|}$, $\frac{D}{|J|}$ and $\frac{K}{|J|}$; correspondingly, the inverse of the temperature scales as $|J|\beta$.

In Appendix B we present the nine possible dimer configurations of neighbouring sites in the chain and their respective energy per unit of $|J|$. The ground state of the ferromagnetic BEG model is composed of dimer states which minimize the energy at $T=0$.

The value of the parameter $\frac{K}{|J|}$ determines the general structure of the $T=0$ phase diagram of the ferromagnetic BEG model.

(i) The case $\frac{K}{|J|} < -1$: The $T=0$ phase diagram for this case is

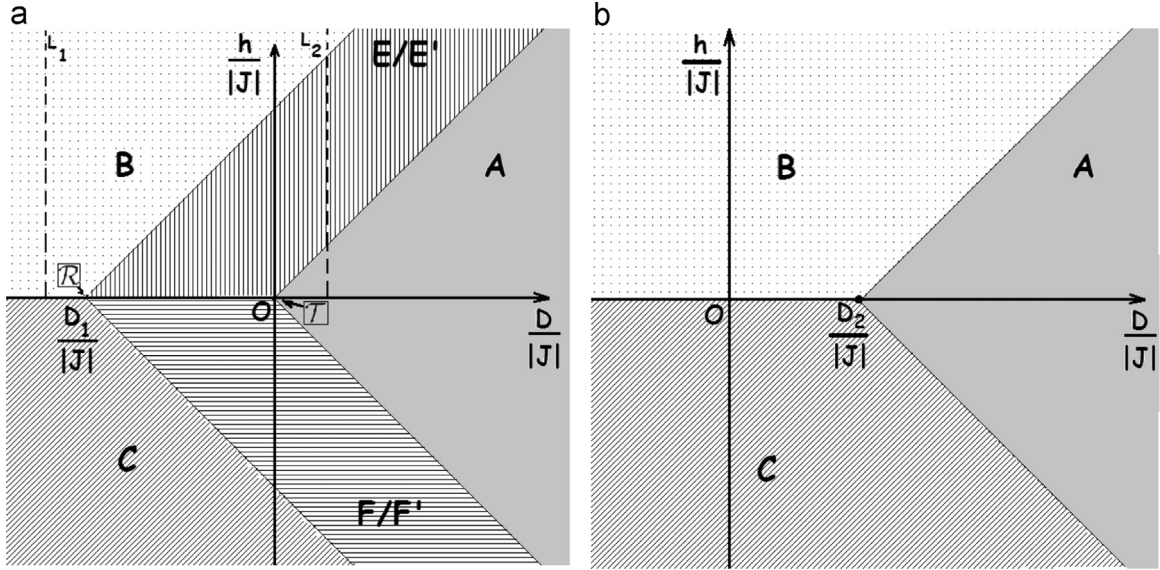


Fig. 1. The phase diagrams, at $T=0$, of the ferromagnetic BEG model in the presence of an external magnetic field. In (a) we have $\frac{K}{J} < -1$. The vector states corresponding to phases A, B, ..., F/F' are given in Appendix C. The multicritical point \mathcal{R} is at $\frac{D_1}{J} = 1 + \frac{K}{J}$. In the phase diagram (b) we have $\frac{K}{J} \geq -1$. The phases A, B and C in this diagram are the same the ones that appear in diagram (a). The tricritical point in this diagram is at $\frac{D_2}{J} = \frac{1}{2} + \frac{K}{2J}$.

represented in Fig. 1a. It resembles the phase diagram of the classical spin-1 AF Ising model with single ion anisotropy term and external longitudinal magnetic field, discussed in Ref. [5]. However, the AF Néel states $|\Psi_0\rangle_C$ and $|\Psi_0\rangle_{C'}$ [cf. [5, Eqs. (C.3a) and (C.3b)]] are naturally absent from Fig. 1a. The ray (half-line) $\frac{h}{|J|} = \frac{D}{|J|}$ extending from the origin separates the phases A and E/E' , whereas the parallel ray $\frac{h}{|J|} = \frac{D}{|J|} - 1 - \frac{K}{J}$, extending from the point $(\frac{D_1}{J}, 0)$, in which $\frac{D_1}{J} = 1 + \frac{K}{J} < 0$, separates the phases E/E' and B. Correspondingly, the ray $\frac{h}{|J|} = -\frac{D}{|J|}$ from the origin separates the phases A and F/F' and the parallel ray $\frac{h}{|J|} = -\frac{D}{|J|} + 1 + \frac{K}{J}$ from $(\frac{D_1}{J}, 0)$ separates the phases F/F' and C. The two rays from the origin and their parallel rays are displaced horizontally by $|\frac{D_1}{J}|$. Such displacement increases as the value of $\frac{K}{J}$ decreases.

The chain states corresponding to each phase are described in the Appendix C of this paper. Those states are represented as $|\Psi_0\rangle_X$, in which $X \in \{A, B, C, E, E', F, F'\}$. The phases $\{A, B, C\}$ correspond to the nondegenerate chain states $|\Psi_0\rangle_A$, $|\Psi_0\rangle_B$ and $|\Psi_0\rangle_C$, respectively [cf. Eqs. (C.1a)–(C.1c)], whereas the phases $\{E/E', F/F'\}$ are twofold degenerate, corresponding to the pairs of chain states $(|\Psi_0\rangle_E, |\Psi_0\rangle_{E'})$ and $(|\Psi_0\rangle_F, |\Psi_0\rangle_{F'})$, respectively [cf. Eqs. (C.1d)–(C.1g)].

The number of degenerate ground states corresponding to the lines and critical points separating the phases in Fig. 1a at $T=0$ can also be calculated. Along one such line, we may determine the possible states of neighboring sites in the chain, which are those dimer states listed in Appendix B that minimize the energy along that line. The same guideline can be applied to the critical points \mathcal{R} and \mathcal{T} . In Appendix D the degeneracy of states on those lines and points for $T=0$ is detailed.

Let $\Omega_{U=V}(T=0)$ be the number of degenerate ground state vectors along the line that separates two distinct phases U and V of the phase diagram in Fig. 1a, excluding the critical points \mathcal{R} and \mathcal{T} . These degenerate states do not necessarily satisfy the periodic spatial boundary condition. Our aim is calculating the entropy per site, at $T=0$, along the lines that separate the distinct phases in the phase diagrams of Fig. 1a and b. In Appendix D we show that the entropy per site along those lines is the same whether we take into account the periodic spatial boundary condition or not. We

obtain

$$\Omega_{B=C}(T=0) = 2, \quad (7a)$$

$$\Omega_{E/E'=F/F'}(T=0) = \frac{3}{4} 2^{\frac{N+1}{2}} \left(1 + (-1)^{N+1} \right) + 2^{\frac{N}{2}} \left(1 + (-1)^N \right), \quad (7b)$$

$$\begin{aligned} \Omega_{A=E/E'}(T=0) &= \Omega_{A=F/F'}(T=0) = \Omega_{B=E/E'}(T=0) \\ &= \Omega_{C=F/F'}(T=0) \\ &= \frac{1}{10} \left(\frac{1+\sqrt{5}}{2} \right)^N (5+3\sqrt{5}) \\ &\quad + \frac{1}{10} \left(\frac{1-\sqrt{5}}{2} \right)^N (5-3\sqrt{5}), \end{aligned} \quad (7c)$$

in which N is the total number of sites in the chain. We are assuming that N is even: $N = 2M$, in which $M \in \mathbb{N}$. Moreover, the number of degenerate ground state vectors at $T=0$, at the critical points \mathcal{R} and \mathcal{T} is given by

$$\Omega_{\mathcal{R}}(T=0) = 3 \times 2^{N-1}, \quad \text{and} \quad (8a)$$

$$\Omega_{\mathcal{T}}(T=0) = \frac{1}{3} \left(2^{N+2} - (-1)^N \right). \quad (8b)$$

Again $\Omega_{\mathcal{R}}$ and $\Omega_{\mathcal{T}}$ are the total number of degenerate ground states at these critical points, including the states that do not satisfy the periodic spatial boundary condition.

Except for the line separating the phases B and C in the phase diagram of Fig. 1a, all other lines are highly degenerate. The results (7a)–(8b) do not depend on the particular value and sign of the exchange strength J ; rather, they depend only on which dimer configurations yield the minimum energy for the parameter scenario along each line. Consequently, a comparison of the phase diagram in Fig. 1a and the phase diagram shown in Fig. 1b of Ref. [5] for the AF spin-1 model with single ion-anisotropy and external longitudinal magnetic field shows that the phases and the lines separating them are the same. Moreover, those lines have the same degeneracy in both diagrams.

(ii) *The case $\frac{K}{J} \geq -1$:* The $T=0$ phase diagram of the ferromagnetic BEG model in this case is shown in Fig. 1b. The lines $\frac{h}{J} = \mp \frac{1}{2} \pm \frac{D}{J} \mp \frac{K}{2J}$, separate the phases A and B, and the phases A and C, respectively. All phases A, B and C are nondegenerate, and they are described by the chain state vectors $|\Psi_0\rangle_A$, $|\Psi_0\rangle_B$ and $|\Psi_0\rangle_C$, respectively.

Appendix B shows the nine possible dimer states and their corresponding energies. Along the horizontal line that separates the phases B and C in Fig. 1b to the point $\frac{D}{J}$, the energies of the dimers $|D^{(B)}\rangle_{i,i+1}$ and $|D^{(C)}\rangle_{i,i+1}$ [cf. (B.2) and (B.3)] are the same and correspond to the minimum value of energy out of the nine possibilities. The chain ground states that can be constructed from $|D^{(B)}\rangle_{i,i+1}$ and $|D^{(C)}\rangle_{i,i+1}$ along that line are $|\Psi_0\rangle_B$ and $|\Psi_0\rangle_C$ [cf. (C.1b) and (C.1c) of Appendix C]. The degree of degeneracy of the ground state along this line is equal to 2.

Likewise, along the line separating the phases A and B in Fig. 1b, the dimer states with minimum energy are $|D^{(A)}\rangle_{i,i+1}$ and $|D^{(B)}\rangle_{i,i+1}$ [cf. (B.1) and (B.2)], and from those the chain ground states correspond to $|\Psi_0\rangle_A$ and $|\Psi_0\rangle_B$ [cf. (C.1a) and (C.1b)]. Hence the degree of degeneracy of the ground state along this line is also equal to 2.

A similar argument holds for the line separating the phases A and C; its degeneracy is also equal to 2.

The existence or not of an exponentially growing degeneracy of the ground states along the separation lines in the phase diagrams of Fig. 1a and b, at $T=0$, determines the thermodynamic behavior of the ferromagnetic BEG model.

3.1. Thermodynamic behavior of the ferromagnetic BEG model

In this subsection we discuss three thermodynamic functions per site of the ferromagnetic ($J < 0$) BEG model: the z-component of the magnetization,

$$\mathcal{M}_z(J, h, D, K; \beta) = -\frac{1}{2} \frac{\partial \mathcal{W}}{\partial h}, \quad (9a)$$

the specific heat

$$C(J, h, D, K; \beta) = -\beta^2 \frac{\partial^2 [\beta \mathcal{W}]}{\partial \beta^2}, \quad (9b)$$

and the entropy

$$S(J, h, D, K; \beta) = \beta^2 \frac{\partial \mathcal{W}}{\partial \beta}, \quad (9c)$$

in which $\mathcal{W}(J, h, D, K; \beta)$ is the HFE of the model. Its exact expression at finite temperature T (in kelvin) can be found in Appendix A.

In the following we let $J = -1$; the remaining parameters in the Hamiltonian (2) are in units of J : $\frac{h}{J}$, $\frac{D}{J}$ and $\frac{K}{J}$. The inverse of temperature β is scaled as $|J|\beta$ in those functions. Our aim is verifying the effect of the degeneracy along the separating lines in the $T=0$ phase diagrams of Fig. 1a and b on these thermodynamic functions. We will discuss separately the regions of the phase diagram in which $\frac{K}{J} < -1$ and $\frac{K}{J} \geq -1$.

The case $\frac{K}{J} < -1$ is exemplified in Fig. 2, which shows $\mathcal{M}_z(\frac{h}{J})$ for $J = -1$ and $\frac{K}{J} = -1.5$. That corresponds to examining, in the phase diagram of Fig. 1a, a vertical straight line in the upper half-plane $\frac{h}{J} \geq 0$. Two scenarios can be qualitatively distinguished. The first scenario is exemplified by Fig. 2a, which shows $\mathcal{M}_z(\frac{h}{J})$ for $\frac{D}{J} = -2$ and $|J|\beta \in \{1.5, 5, 100\}$. This figure corresponds to following upwards the vertical line L_1 in the phase diagram in Fig. 1a, which begins at the point corresponding to $\frac{D}{J} = -2$ and $h=0$, on the horizontal axis. Along the vertical line L_1 , the degree of degeneracy of the ground state vector is 2. Fig. 2a shows that for ($J = -1$, $\frac{K}{J} = -1.5$ and $\frac{D}{J} = -2$), the step-function shape of $\mathcal{M}_z(\frac{h}{J})$ is lost about $|J|\beta = 1.5$. The second scenario is exemplified by Fig. 2b, which shows $\mathcal{M}_z(\frac{h}{J})$ for $\frac{D}{J} = 0.25$ and $|J|\beta \in \{10, 100, 1000\}$. It corresponds to following upwards the vertical line L_2 in the phase diagram in Fig. 1a, starting from the point corresponding to $\frac{D}{J} = 0.25$ and $h=0$, on the horizontal axis. L_2 intersects two phase transition lines: from A to E/E' at $\frac{h}{J} = 0.25$ and from E/E' to B at $\frac{h}{J} = 0.75$. The degeneracies of the ground state vectors along these two transition lines are exponential [cf. Eq. (7c)]. Consequently, the shape of the curve $\mathcal{M}_z(\frac{h}{J})$ at $|J|\beta = 10$ is quite distinct from that of the corresponding curve at $|J|\beta = 1000$. For the latter, the z-component of the magnetization has two plateaux that resemble quite closely a sequence of step-functions. At $|J|\beta = 10$, however, the plateaux are no longer present. That same behavior of $\mathcal{M}_z(\frac{h}{J})$ for

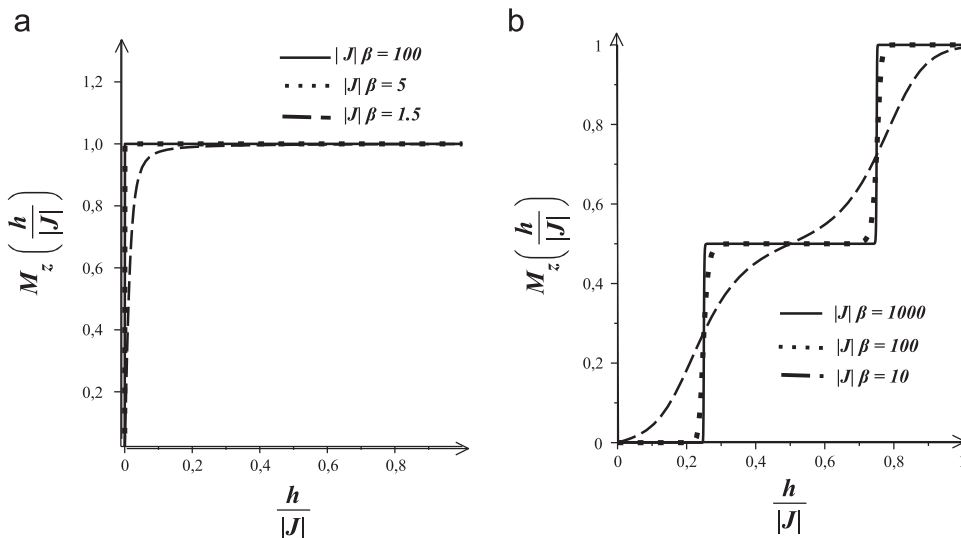


Fig. 2. The z-component of the magnetization \mathcal{M}_z per site as a function of the external magnetic field $\frac{h}{J}$ for the ferromagnetic BEG model. In (a), \mathcal{M}_z is shown for $\frac{D}{J} = -2$ and several values of $|J|\beta$: 100 (solid line), 5 (dotted line) and 1.5 (dashed line). In (b) we have $\frac{D}{J} = 0.25$ with the curves plotted for distinct values of $|J|\beta$: 1000 (solid line), 100 (dotted line) and 10 (dashed line). In both figures we have $J = -1$ and $\frac{K}{J} = -1.5$.

different temperatures is seen in any curve for $\frac{D}{J} > \frac{D_1}{J_1}$, in which $\frac{D_1}{J_1} = 1 + \frac{K}{J_1}$, and $\frac{K}{J_1} < -1$.

Fig. 3 shows the function $M_z(\frac{h}{J})$ for $\frac{K}{J_1} \geq -1$. In Fig. 3a and b we have $J = -1$ (ferro) and $\frac{K}{J_1} = 1$. In Fig. 3a we choose $\frac{D}{J_1} = -0.5$. The vertical line in the phase diagram of Fig. 1b followed by the argument $\frac{h}{J_1}$ of the function M_z , begins at $\frac{D}{J_1} = -0.5$ with $h=0$ and crosses the phase B of this diagram at $T=0$. From Fig. 3a we see that the function $M_z(\frac{h}{J_1})$ has the plateau $M_z = 1$ up to $|J|\beta \sim 5$. For $|J|\beta = 1.5$ the curve $M_z(\frac{h}{J_1})$ in Fig. 3a differs from the step-function around $\frac{h}{J_1} \sim 0$. One is reminded that the degeneracy of the ground state vectors along the line that separates the phases B and C in Fig. 1b is equal to 2.

In Fig. 3b we have $\frac{D}{J_1} = 1.8$. The function $M_z(\frac{h}{J_1})$ is plotted for the variable $\frac{h}{J_1}$ varying along the vertical line in the phase diagram 1b with $\frac{D}{J_1} = 1.8$. This vertical line crosses the phase A and cut the line that separates the phases A and B in the phase diagram 1b at $\frac{h}{J_1} = 0.8$, going along the phase B. The number of degenerate ground state vectors along the line separating the phases A and B in the phase diagram is equal to 2. In Fig. 3b the curves of the function $M_z(\frac{h}{J_1})$ have two plateaux, $M_z = 0$ and $M_z = 1$, for $|J|\beta$ up to 5. It loses the step-function form for $|J|\beta \sim 1.5$ (a high temperature $T \sim \frac{2|J|}{3}$). Comparing the curves of the z-component of the magnetization as a function of the $\frac{h}{J_1}$ in Figs. 2a, 3a and b, we verify that the plateaux in those curves are present up to a high enough temperature. The common fact about these three curves is that the vertical line in the phase diagrams of Fig. 1 (for an increasing value of $\frac{h}{J_1}$ and a steady value of $\frac{D}{J_1}$) cut phase transition lines for which the degeneracy of the ground state vectors are not exponential.

The entropy per site $S(J, h, D, K; \beta)$ can be derived from the HFE $\mathcal{W}(J, h, D, K; \beta)$ of the model through the relation between these two functions presented previously, see Eq. (9c), or through the number of states with energy between E and $E + \delta E$, with $\delta E \ll E$ [13], $\Omega(\bar{E})$, in the thermodynamic limit,

$$S(J, h, D, K; \beta) = \lim_{N \rightarrow \infty} \frac{k}{N} \ln(\Omega(\bar{E})). \quad (10)$$

From this point on, we will use a system of units in which $k=1$.

Using an algebraic manipulation program we derive from the results of Appendix A the temperature dependence of the entropy per site of the BEG model (ferromagnetic and AF models), valid for $T > 0$. In Eqs. (7a)–(8b) we present the number of degenerate ground state vectors along the line that separate the different phases in the diagrams 1a and b, at $T=0$, and the critical points \mathcal{R} and \mathcal{T} .

By varying the inverse of temperature, $|J|\beta$, up to 10^7 , we verify numerically that the entropy per site, $S(-1, \frac{h}{J_1}, \frac{D}{J_1}, \frac{K}{J_1}; |J|\beta)$, has a strong indication that the limit of this thermodynamic function as $T \rightarrow 0$ ($|J|\beta \rightarrow \infty$) along the lines that separate the phases in Fig. 1a and b are as follows.

(1) For $\frac{K}{J_1} < -1$ (phase diagram 1a) we have, for the $B \rightleftharpoons C$ transition line,

$$\lim_{|J|\beta \rightarrow \infty} S_{B \rightleftharpoons C} \left(-1, 0, \frac{D}{J_1}, \frac{K}{J_1}; |J|\beta \right) = \lim_{N \rightarrow \infty} \frac{1}{N} \ln(\Omega_{B \rightleftharpoons C}(T=0)) = 0, \quad (11a)$$

with $\frac{D}{J_1} < \frac{D_1}{J_1}$ and $\frac{D_1}{J_1} = 1 + \frac{K}{J_1}$. For the $E/E' \rightleftharpoons F/F'$ transition line,

$$\begin{aligned} \lim_{|J|\beta \rightarrow \infty} S_{E/E' \rightleftharpoons F/F'} \left(-1, 0, \frac{D}{J_1}, \frac{K}{J_1}; |J|\beta \right) \\ = \lim_{N \rightarrow \infty} \frac{1}{N} \ln(\Omega_{E/E' \rightleftharpoons F/F'}(T=0)) = \frac{1}{2} \ln(2) \approx 0.3466, \end{aligned} \quad (11b)$$

with $\frac{D_1}{J_1} < \frac{D}{J_1} < 0$. For the $B \rightleftharpoons E/E'$ transition line,

$$\begin{aligned} \lim_{|J|\beta \rightarrow \infty} S_{B \rightleftharpoons E/E'} \left(-1, \frac{h}{J_1}, \frac{D}{J_1}, \frac{K}{J_1}; |J|\beta \right) \\ = \lim_{|J|\beta \rightarrow \infty} S_{C \rightleftharpoons F/F'} \left(-1, \frac{h}{J_1}, \frac{D}{J_1}, \frac{K}{J_1}; |J|\beta \right) \\ = \lim_{N \rightarrow \infty} \frac{1}{N} \ln(\Omega_{B \rightleftharpoons E/E'}(T=0)) \\ = \lim_{N \rightarrow \infty} \frac{1}{N} \ln(\Omega_{C \rightleftharpoons F/F'}(T=0)) = \ln\left(\frac{1+\sqrt{5}}{2}\right) \approx 0.4812, \end{aligned} \quad (11c)$$

with $\frac{h}{J_1} = \pm \frac{D}{J_1} \mp 1 \mp \frac{K}{J_1}$ and $\frac{D}{J_1} > \frac{D_1}{J_1}$. For the $A \rightleftharpoons E/E'$ transition line,

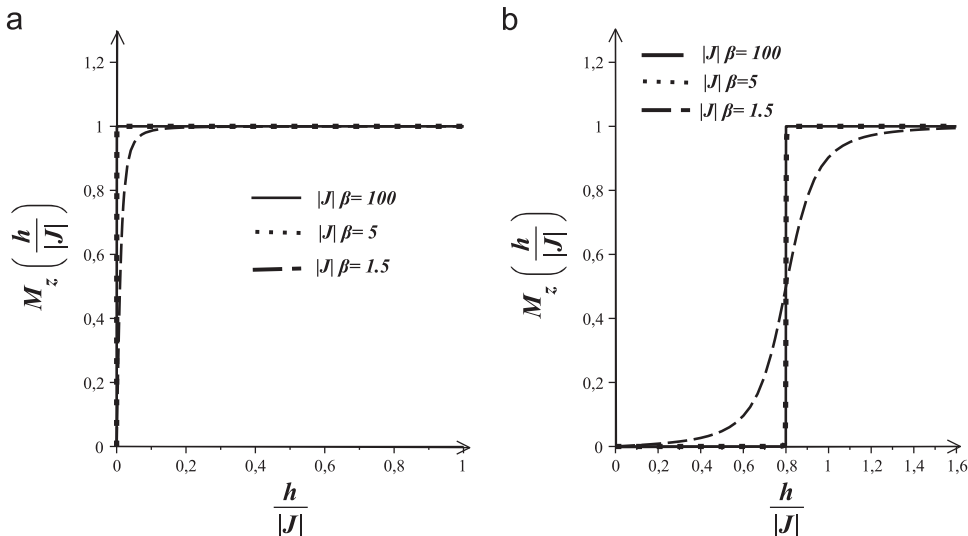


Fig. 3. The z-component of the magnetization M_z per site as a function of the external magnetic field $\frac{h}{J_1}$ for the ferromagnetic BEG model in the region $\frac{K}{J_1} \geq -1$. In (a) we take $\frac{D}{J_1} = -0.5$. The curves are plotted for different values of $|J|\beta$: 100 (solid line), 5 (dotted line) and 1.5 (dashed line). In (b) we have $\frac{D}{J_1} = 1.8$ and M_z is plotted for three values of $|J|\beta$: 1000 (solid line), 100 (dotted line) and 10 (dashed line). In (a) and (b) we take $J = -1$ and $\frac{K}{J_1} = 1$.

$$\begin{aligned}
\lim_{|J|\beta \rightarrow \infty} S_{A=E/E'} \left(-1, \frac{h}{|J|}, \frac{D}{|J|}, \frac{K}{|J|}; |J|\beta \right) \\
= \lim_{|J|\beta \rightarrow \infty} S_{A=F/F'} \left(-1, \frac{h}{|J|}, \frac{D}{|J|}, \frac{K}{|J|}; |J|\beta \right) \\
= \lim_{N \rightarrow \infty} \frac{1}{N} \ln(\Omega_{A=E/E'}(T=0)) = \lim_{N \rightarrow \infty} \frac{1}{N} \ln(\Omega_{A=F/F'}(T=0)) \\
= \ln \left(\frac{1 + \sqrt{5}}{2} \right) \approx 0.4812,
\end{aligned} \quad (11d)$$

with $\frac{h}{|J|} = \pm \frac{D}{|J|}$ and $\frac{D}{|J|} > 0$.

In the multicritical points \mathcal{R} and \mathcal{T} , at $T=0$, we have the limits:

$$\begin{aligned}
\lim_{|J|\beta \rightarrow \infty} S_{\mathcal{R}} \left(-1, 0, \frac{D_1}{|J|}, \frac{K}{|J|}; |J|\beta \right) &= \lim_{|J|\beta \rightarrow \infty} S_{\mathcal{T}} \left(-1, 0, 0, \frac{K}{|J|}; |J|\beta \right) \\
&= \lim_{N \rightarrow \infty} \frac{1}{N} \ln(\Omega_{\mathcal{R}}(T=0)) \\
&= \lim_{N \rightarrow \infty} \frac{1}{N} \ln(\Omega_{\mathcal{T}}(T=0)) = \ln(2) \\
&\approx 0.6931,
\end{aligned} \quad (11e)$$

where $\frac{D}{|J|} = \frac{D_1}{|J|} = 1 + \frac{K}{|J|}$ (point \mathcal{R}) or $\frac{D}{|J|} = 0$ (point \mathcal{T}).

(2) For $\frac{K}{|J|} \geq 1$ (phase diagram 1b) we also vary the inverse of the temperature, $|J|\beta$, in the interval $[0, 10^8]$, and the results strongly indicate that

$$\lim_{|J|\beta \rightarrow \infty} S \left(-1, \frac{h}{|J|}, \frac{D}{|J|}, \frac{K}{|J|}; |J|\beta \right) = 0, \quad (12)$$

for any value for the parameters $\frac{h}{|J|}, \frac{D}{|J|}$, when $\frac{K}{|J|} \geq -1$.

Fig. 4 represents the entropy per site as a function of $\frac{D}{|J|}$ for $\frac{K}{|J|} = -1.5$ at $|J|\beta = 10^3$. The twin peaks in the curve correspond to the points \mathcal{R} ($\frac{D}{|J|} = -0.5$) and \mathcal{T} ($\frac{D}{|J|} = 0$) in the phase diagram 1b. Since $T > 0$ for this picture, the curve is continuous everywhere. We verify that at low temperature the points \mathcal{R} and \mathcal{T} are well featured in the curve $S \times \frac{D}{|J|}$.

The relation $\frac{C(T)}{T} = \frac{\partial S(T)}{\partial T}$ connects the specific heat per site, in

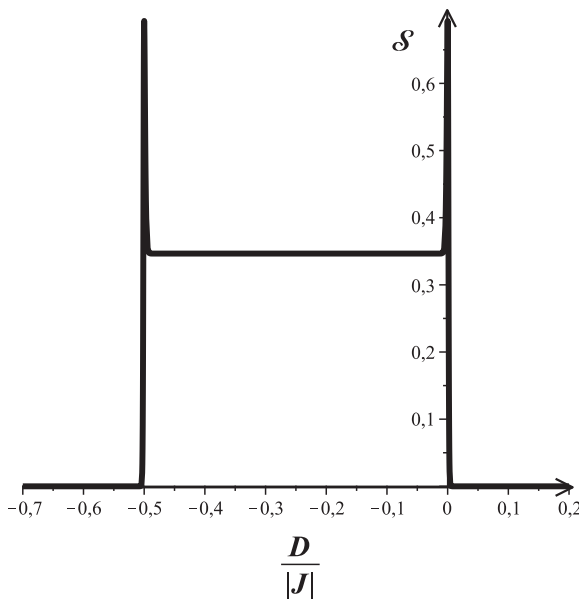


Fig. 4. The entropy per site S as a function of the single-ion parameter $\frac{D}{|J|}$ is shown at $|J|\beta = 10^3$, with $\frac{K}{|J|} = -1.5$ and $\frac{h}{|J|} = 0$. We vary the parameter $\frac{D}{|J|}$ along the horizontal line $\frac{h}{|J|} = 0$ in phase diagram of Fig. 1a in order to include in the curve the critical points, at $T=0$, \mathcal{R} ($\frac{D}{|J|} = -0.5$) and \mathcal{T} ($\frac{D}{|J|} = 0$).

units of the temperature, and the variation of the entropy per site with the temperature. In what follows we will discuss the behavior of the specific heat per site in the two regions of the parameter $\frac{K}{|J|}$: $\frac{K}{|J|} < -1$ and $\frac{K}{|J|} \geq -1$.

For $\frac{K}{|J|} < -1$ and $\frac{D}{|J|} < 1 + \frac{K}{|J|}$, the maximum value of the specific heat per site, as function of $\frac{h}{|J|}$ at $|J|\beta = 10^2$, is of order 10^{-85} . For this set of values of the parameters $\frac{D}{|J|}$ and $\frac{K}{|J|}$, increasing the variable $\frac{h}{|J|}$ corresponds to following a vertical line in the phase diagram 1a that does not cut any line in the diagram that has an exponential degeneracy in the ground state at $T=0$. The maximum value of $C(\frac{h}{|J|})$ at $|J|\beta = 10$ is of order 10^{-7} and at $|J|\beta = 2$ the highest value of this thermodynamic function is of order 10^{-2} . For the temperature varying two orders of magnitude the specific heat per site varies 10^{83} orders of magnitude.

The specific heat per site with $\frac{K}{|J|} \geq -1$ and $\frac{D}{|J|} \in \mathbb{R}$ has the same behavior as described in the previous paragraph. The phase diagram of the chain with $\frac{K}{|J|} \geq -1$ has no line in which the ground state is exponentially degenerate at $T=0$.

In Fig. 5 the curve $C \times \frac{h}{|J|}$ is drawn with $\frac{K}{|J|} = -1.5$ and $\frac{D}{|J|} = 0.25$.

The variable $\frac{h}{|J|} \geq 0$ follows a vertical line in the phase diagram 1a, at $T=0$, that crosses two lines that separate the phases A and E/E' at $\frac{h}{|J|} = 0.25$, and E/E' and B at $\frac{h}{|J|} = 0.75$. Along these two lines that separate these phases in diagram 1a, the ground state vectors are exponentially degenerate at $T=0$. In Fig. 5a and b the curve $C(\frac{h}{|J|})$ is plotted at $|J|\beta = 10^3$, but in two intervals of the variable $\frac{h}{|J|}$ where this thermodynamic function is non-null at this temperature. In Fig. 5c the specific heat per site is drawn at $|J|\beta = 10$.

We verify from the Fig. 5 that the maximum value of the function $C(\frac{h}{|J|})$ at $|J|\beta = 10^3$ is of the same order of magnitude as at $|J|\beta = 10$. The curve of the specific heat per site as a function of $\frac{h}{|J|}$ at different temperatures, has the same behavior as described in Fig. 5 when $\frac{K}{|J|} < -1$ and $\frac{D}{|J|} > 1 + \frac{K}{|J|}$.

4. Ferromagnetic BEG model at $\frac{K}{|J|} = -1 \times$ AF Ising model at low temperature

Ref. [5] presents the phase diagram of the spin-1 AF Ising model, with single-ion anisotropy term, in the presence of a longitudinal external magnetic field, at $T=0$ (see Fig. 6a). In Fig. 6b we have the phase diagram, also at $T=0$, of the ferromagnetic BEG model with $\frac{K}{|J|} = -2$, in the presence of an external longitudinal magnetic field. Comparing the phase diagrams of these two models, we verify that for $\frac{D}{|J|} > \frac{1}{2}$ the two models have the same phases at $T=0$. The line l_1 in the diagram 6b corresponds to the vertical line $\frac{D}{|J|} = \frac{1}{2}$. (Having the same phases for $\frac{D}{|J|} > \frac{1}{2}$, however, is not a sufficient condition for the existence of a transformation that maps one model onto the other.)

In Section 3.1 we discussed the degeneracy of the ground state along the phase separating lines in the diagram of the ferromagnetic BEG model, at $T=0$, concluding that the results (7a)–(7c) are independent of the sign of J . A analogous discussion for the spin-1 AF Ising model (see Fig. 6a) has not been done in Ref. [5], though.

The independence of the number of degenerate ground states with respect to the sign of the exchange strength J , calculated in Section 3.1, permits us to affirm that the degeneracy of the ground state of the spin-1 AF Ising model along the lines $\frac{h}{|J|} = \pm \frac{D}{|J|}$ with $\frac{D}{|J|} > \frac{1}{2}$ in diagram (Fig. 6a), at $T=0$, is equal to the result (7c). Again

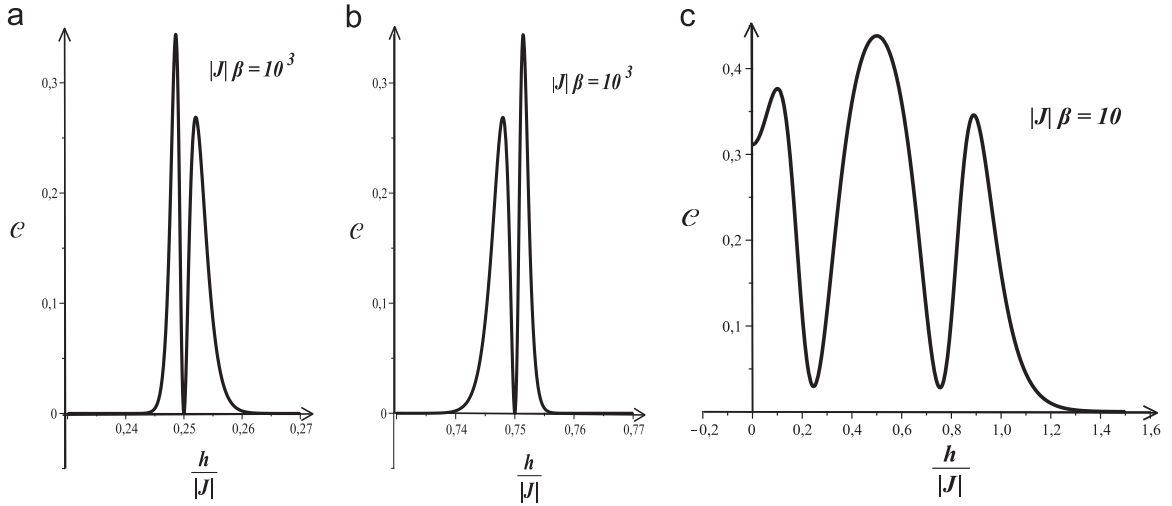


Fig. 5. The specific heat per site C of the ferromagnetic BEG model as a function of the external magnetic field $\frac{h}{|J|}$, with: $J = -1$, $\frac{K}{|J|} = -1.5$ and $\frac{D}{|J|} = 0.25$. In (a) and (b) we take $|J|\beta = 10^3$ and consider the variable $\frac{D}{|J|}$ in two intervals: $[0.23, 0.27]$ and $[0.73, 0.77]$, respectively. Off these intervals the specific heat per site is null at this temperature. In (c), the function $C(\frac{h}{|J|})$ is plotted at $|J|\beta = 10$.

we are also including the states that do not satisfy the periodic spatial boundary condition. The degeneracy of the ground state of the spin-1 AF Ising model, at $T=0$, along the line $\frac{h}{|J|} = \pm 1 \pm \frac{D}{|J|}$, with $\frac{D}{|J|} > 0$, in the phase diagram (Fig. 6a) is equal to result (7b), under the same situation on the spatial boundary condition.

There are phase transitions at $T=0$ in the phase diagram (Fig. 6a) of the spin-1 AF Ising model that are absent in the ferromagnetic BEG model with $\frac{K}{|J|} = -2$. In the following we present the total number of ground states along the lines that separate the phases in the spin-1 AF Ising model. These degenerate ground states do not necessarily satisfy periodic spatial boundary conditions:

$$\Omega_{A=G/G'}^{AF}(T=0) = 3, \quad (13a)$$

$$\begin{aligned} \Omega_{G/G'=E/E'}^{AF}(T=0) &= \Omega_{G/G'=F/F'}^{AF}(T=0) \\ &= 2^{\frac{N+2}{2}} \left(\frac{1 + (-1)^N}{2} \right) \\ &\quad + (2^{\frac{N+1}{2}} + 2^{\frac{N-1}{2}}) \left(\frac{1 + (-1)^{N+1}}{2} \right). \end{aligned} \quad (13b)$$

$$\begin{aligned} \Omega_{B=G/G'}^{AF}(T=0) &= \Omega_{C=G/G'}^{AF}(T=0) \\ &= \left(1 + \frac{2\sqrt{5}}{5} \right) \left(1 + \frac{\sqrt{5}}{2} \right)^{N-1} \\ &\quad + \left(1 - \frac{2\sqrt{5}}{5} \right) \left(1 - \frac{\sqrt{5}}{2} \right)^{N-1}. \end{aligned} \quad (13c)$$

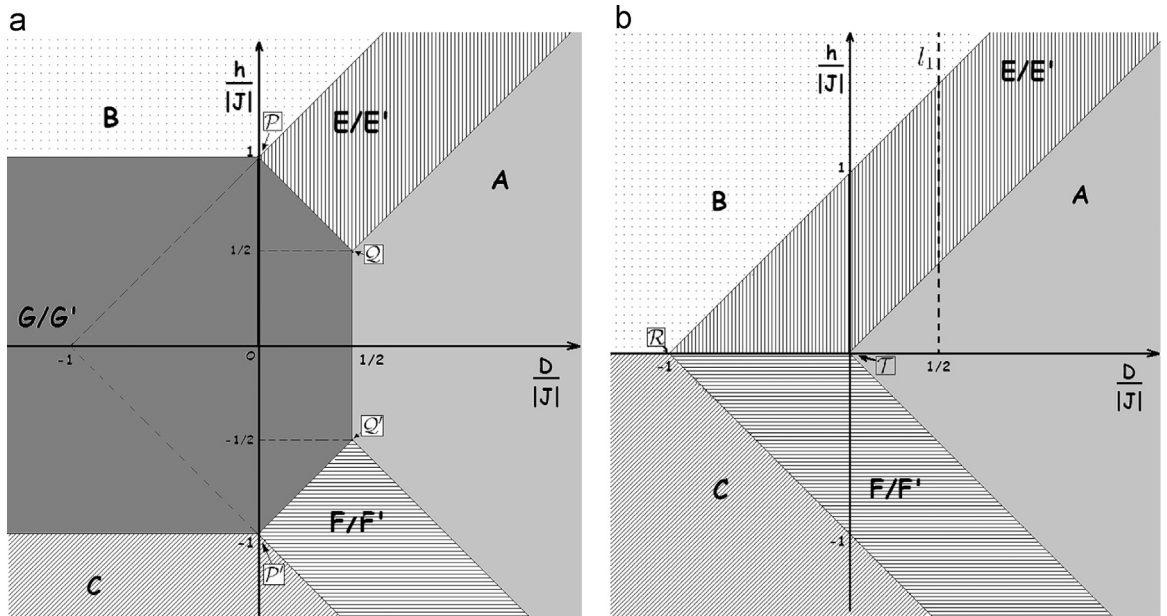


Fig. 6. In (a), the phase diagram of the spin-1 AF Ising model, with single-ion anisotropy term, in the presence of a longitudinal external magnetic field [5], at $T=0$. In (b), the phase diagram 1a of the ferromagnetic BEG model, with $\frac{K}{|J|} = -2$, in the presence of a longitudinal magnetic field at $T=0$.

The number of degenerate ground states at the critical points (\mathcal{P} , \mathcal{P}') in the phase diagram (Fig. 6a) is

$$\Omega_{\mathcal{P}}^{AF} = \Omega_{\mathcal{P}'}^{AF} = \frac{2^{N+2}}{3} + \frac{(-1)^{N+1}}{3}. \quad (14)$$

We do not show here (the lengthy expression of) the number of degenerate ground states at the critical points (\mathcal{Q} , \mathcal{Q}') in the phase diagram (Fig. 6a) of the spin-1 AF Ising model, at $T=0$. Its calculation has been done with the help of a computer algebra system; the interested reader may contact the authors for an ASCII file with that expression.

The entropy per site of these lines in the phase diagram of the spin-1 AF Ising model in Fig. 6a, in the thermodynamic limit ($N \rightarrow \infty$), is

$$\begin{aligned} \lim_{|J|\beta \rightarrow \infty} S_{B \equiv G/G}^{AF} \left(1, \frac{h}{|J|}, \frac{D}{|J|} = \frac{1}{2}, \frac{K}{|J|} = 0; |J|\beta \right) \\ = \lim_{|J|\beta \rightarrow \infty} S_{C \equiv G/G}^{AF} \left(1, \frac{h}{|J|}, \frac{D}{|J|} = \frac{1}{2}, \frac{K}{|J|} = 0; |J|\beta \right) \\ = \ln \left(\frac{1 + \sqrt{5}}{2} \right) \approx 0.4812 \end{aligned} \quad (15a)$$

$$= \lim_{|J|\beta \rightarrow \infty} S_{A \equiv E/E'} \left(-1, \frac{h}{|J|}, \frac{D}{|J|}, \frac{K}{|J|}; |J|\beta \right), \quad (15b)$$

with $\frac{K}{|J|} < -1$ and $\frac{D}{|J|} > 0$. We also have

$$\begin{aligned} \lim_{|J|\beta \rightarrow \infty} S_{E/E' \equiv G/G}^{AF} \left(1, \frac{h}{|J|}, \frac{D}{|J|}, \frac{K}{|J|} = 0; |J|\beta \right) \\ = \lim_{|J|\beta \rightarrow \infty} S_{F/F' \equiv G/G}^{AF} \left(1, \frac{h}{|J|}, \frac{D}{|J|}, \frac{K}{|J|} = 0; |J|\beta \right) \\ = \frac{1}{2} \ln(2) \approx 0.3466 \end{aligned} \quad (16a)$$

$$= \lim_{|J|\beta \rightarrow \infty} S_{E/E' \equiv F/F'} \left(-1, \frac{h}{|J|}, \frac{D}{|J|}, \frac{K}{|J|}; |J|\beta \right). \quad (16b)$$

In the phase diagram of the spin-1 AF Ising model we have $\frac{1}{2} < \frac{h|J|}{|J|} < 1$ and $0 < \frac{D}{|J|} < \frac{1}{2}$. In the phase diagram of the ferromagnetic BEG model, at $T=0$, we have $\frac{K}{|J|} < -1$.

The entropy per site of the critical points (\mathcal{P} , \mathcal{P}'), in the thermodynamic limit ($N \rightarrow \infty$) at $T=0$, is

$$\begin{aligned} \lim_{|J|\beta \rightarrow \infty} S_{\mathcal{P}, \mathcal{P}'}^{AF} \left(1, \frac{h}{|J|} = \pm 1, \frac{D}{|J|} = 0, \frac{K}{|J|} = 0; |J|\beta \right) \\ = \ln(2) \approx 0.6931 \end{aligned} \quad (17a)$$

$$\begin{aligned} &= \lim_{|J|\beta \rightarrow \infty} S_{E/E' \equiv F/F'} \left(-1, \frac{h}{|J|}, \frac{D}{|J|}, \frac{K}{|J|}; |J|\beta \right) \\ &= \lim_{|J|\beta \rightarrow \infty} S_{\mathcal{T}} \left(-1, \frac{h}{|J|} = 0, \frac{D}{|J|} = 0, \frac{K}{|J|}; |J|\beta \right) \\ &= \lim_{|J|\beta \rightarrow \infty} S_{\mathcal{R}} \left(-1, \frac{h}{|J|} = 0, \frac{D_1}{|J|}, \frac{K}{|J|}; |J|\beta \right), \end{aligned} \quad (17b)$$

where $\frac{D_1}{|J|} = 1 + \frac{K}{|J|}$, with $\frac{K}{|J|} < -1$. We also have at the critical points (\mathcal{Q} , \mathcal{Q}')

$$\lim_{|J|\beta \rightarrow \infty} S_{\mathcal{Q}, \mathcal{Q}'}^{AF} \left(1, \frac{h}{|J|} = \pm \frac{1}{2}, \frac{D}{|J|} = \frac{1}{2}, \frac{K}{|J|} = 0; |J|\beta \right) \approx 0.5886. \quad (18)$$

The quantity $\lim_{|J|\beta \rightarrow \infty} S_{\mathcal{Q}, \mathcal{Q}'}^{AF}$ can be obtained with arbitrary precision.

The previous information about the degeneracy of the ground

state of the spin-1 Ising model at $T=0$ and along the lines that separate the phases in the diagram (Fig. 6a), complements the information of Ref. [5] about the phase diagram of the spin-1 AF Ising model, with single-ion anisotropy term and in the presence of an external longitudinal magnetic field, at $T=0$.

Let us examine in what follows the consequences of having the same phase diagram at $T=0$ for $\frac{D}{|J|} > \frac{1}{2}$ (see the diagrams of Fig. 6), in the presence of an external longitudinal magnetic field, for both the ferromagnetic BEG model (with $\frac{K}{|J|} = -2$) and the spin-1 AF Ising model with single-ion anisotropy term (with $\frac{K}{|J|} = 0$).

At very low temperature, the contribution to the thermodynamic functions of a model comes mainly from its ground state, degenerate or not. In the following we compare the z -component of the magnetization, specific heat and entropy *per site* [in Eqs. (9a), (9b) and (9c), respectively] of both models at $|J|\beta = 500$ and $|J|\beta = 100$. At the latter temperature, we expect that the excited states of the models give contribution to the thermodynamic functions due to the exponential degeneracy of these states in each model.

The big difference between the ferromagnetic BEG model, under consideration in this section, and the spin-1 AF Ising model is the sign of the exchange strength J . In the former (latter) model we have $J = -1$ ($J=1$). We notice from the Hamiltonians (1) and (2) that in order to compare the contribution of the J -term to the partition function of the model and the contributions from the external longitudinal magnetic field and the single-ion anisotropy term, we have to compare the values of the parameters: J , $2h$ and $2D$.

For a fixed value of $\frac{D}{|J|} > \frac{1}{2}$, we have varied the external longitudinal magnetic field in whole interval, that is, $\frac{h}{|J|} \in [0, \infty)$ and have compared the three thermodynamic functions mentioned previously.

Along the vertical line in the phase diagrams of Fig. 6, with fixed value of $\frac{D}{|J|}$, we have an interval of $\frac{h}{|J|} \in [0, \frac{D}{|J|})$ for which M_z vanishes at $|J|\beta = 500$ and $|J|\beta = 100$. In order to avoid any singular point in this comparison we define the difference of these functions as

$$\begin{aligned} \text{Diff}(M_z)_{Fe}^{AF} \left(\frac{h}{|J|}, \frac{D}{|J|}; |J|\beta \right) \\ \equiv M_z^{Fe} \left(-1, \frac{h}{|J|}, \frac{D}{|J|}, \frac{K}{|J|} = -2; |J|\beta \right) \\ - M_z^{AF} \left(1, \frac{h}{|J|}, \frac{D}{|J|}, \frac{K}{|J|} = 0; |J|\beta \right). \end{aligned} \quad (19)$$

Fig. 7a shows the magnetization difference (19) as a function of $\frac{h}{|J|}$ for $\frac{D}{|J|} = 0.51$ and $|J|\beta = 500$, in an interval about $\frac{h}{|J|} \sim 0.51$ with amplitude of order 10^{-10} , in which the transition $A \rightleftharpoons E/E'$ occurs. For $\frac{h}{|J|} \gtrsim 0.511$, the difference (19) of the functions M_z is a monotonically decreasing function, where we have:

$$\text{Diff}(M_z)_{Fe}^{AF} \left(\frac{h}{|J|} = 0.52, \frac{D}{|J|} = 0.51; |J|\beta = 500 \right) \approx 4.6 \times 10^{-14}, \quad (20a)$$

$$\text{Diff}(M_z)_{Fe}^{AF} \left(\frac{h}{|J|} = 1, \frac{D}{|J|} = 0.51; |J|\beta = 500 \right) \approx 1.6 \times 10^{-222}, \quad (20b)$$

$$\text{Diff}(M_z)_{Fe}^{AF} \left(\frac{h}{|J|} = 1.51, \frac{D}{|J|} = 0.51; |J|\beta = 500 \right) \approx 3.8 \times 10^{-444}. \quad (20c)$$

One is reminded that at $\frac{h}{|J|} = 1.51$ we have the phase transition $B \rightleftharpoons E/E'$ in the phase diagrams of Fig. 6, at $T=0$.

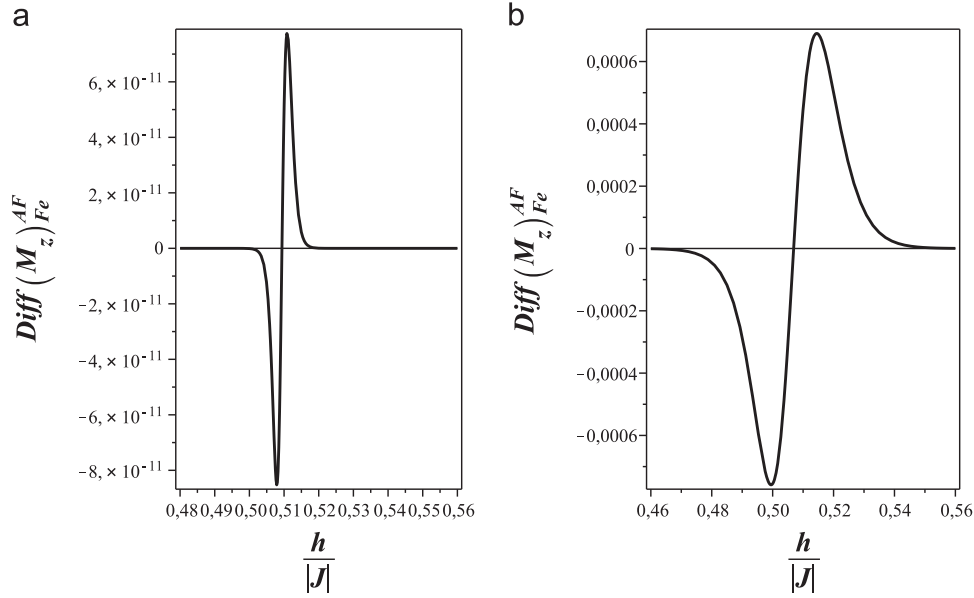


Fig. 7. The difference (19) between the z-component of the magnetization, M_z , as a function of the external magnetic field $\frac{h}{J}$, of the ferromagnetic BEG model with $\frac{K}{J} = -2$, and the spin-1 AF Ising model, with single-ion anisotropy term. In (a) that difference is shown for $J|\beta = 500$; in (b), for $J|\beta = 100$.

Keeping $\frac{D}{J} = 0.51$ and increasing the temperature to $J|\beta = 100$, the difference of the z-components of the magnetization of the two models decreases; it is shown in Fig. 7b. For $\frac{h}{J} \sim 0.51$, the value of the parameter $\frac{2h}{J}$ is close to 1 and the ferro- or anti-ferromagnetic nature of the models begins to appear. For $\frac{h}{J} \gtrsim 0.516$, the function $\text{Diff}(M_z)_{Fe}^{AF}$ is a monotonically decreasing function of the external magnetic field $\frac{h}{J}$ and

$$\text{Diff}(M_z)_{Fe}^{AF}\left(\frac{h}{J} = 1, \frac{D}{J} = 0.51; J|\beta = 100\right) \approx 2.5 \times 10^{-45}, \quad (21a)$$

$$\text{Diff}(M_z)_{Fe}^{AF}\left(\frac{h}{J} = 1.51, \frac{D}{J} = 0.51; J|\beta = 100\right) \approx 9.2 \times 10^{-90}. \quad (21b)$$

For $\frac{D}{J} = 1$ we obtain that the difference (19) of the z-component of the magnetization of the two aforementioned models at $J|\beta = 500$ is $|\text{Diff}(M_z)_{Fe}^{AF}| \lesssim 10^{-436}$ in the interval of $\frac{h}{J} \in [0.98, 1.05]$ and $|\text{Diff}(M_z)_{Fe}^{AF}| \lesssim 10^{-825}$ in the interval of $\frac{h}{J} \in [1.9, 2.1]$. For $J|\beta = 100$ these differences decrease and they are $\lesssim 10^{-89}$. Increasing the value of $\frac{D}{J}$ (crystal field per unit of J) it is impossible to experimentally measure the difference between the z-component of the ferro ($J = -1$) and AF ($J = 1$) models.

In order to compare the specific heat and the entropy, both per site, of ferromagnetic BEG model with $\frac{K}{J} = -2$ and the spin-1 AF Ising model, we define the percent differences

$$PD(L)_{Fe}^{AF}\left(\frac{h}{J}, \frac{D}{J}; J|\beta\right) \equiv \left(\frac{L_{Fe}^{BEG}\left(-1, \frac{h}{J}, \frac{D}{J}, \frac{K}{J} = -2; J|\beta\right) - L_{AF}^{Ising}\left(1, \frac{h}{J}, \frac{D}{J}, \frac{K}{J} = 0; J|\beta\right)}{L_{Fe}^{BEG}\left(-1, \frac{h}{J}, \frac{D}{J}, \frac{K}{J} = -2; J|\beta\right)} \right) \times 100\%, \quad (22)$$

where L can be the specific heat per site, C , or the entropy per site, S .

First, let us compare the specific heat per site of the two models. First we consider $\frac{D}{J} = 0.51$ at $J|\beta = 500$. We obtain that

$|PD(C)_{Fe}^{AF}| \lesssim 10^{-6}\%$ in the interval $\frac{h}{J} \in [0, 0.5]$, but at $\frac{h}{J} = 0.51$, in which occurs the $A \rightleftharpoons E/E'$ transition in the diagrams of Fig. 6, at $T=0$, the value of the specific heat per site at each model is

$$C_{Fe}^{BEG}\left(-1, \frac{h}{J} = 0.51, \frac{D}{J} = 0.51, \frac{K}{J} = -2; J|\beta = 500\right) \approx 3.04 \times 10^{-213} \quad (23a)$$

$$C_{AF}^{Ising}\left(1, \frac{h}{J} = 0.51, \frac{D}{J} = 0.51, \frac{K}{J} = 0; J|\beta = 500\right) \approx 8.70 \times 10^{-8}, \quad (23b)$$

showing a difference of 205 orders of magnitude in the specific heat per site of the two models. We do not know which mechanism permits so huge difference between these two thermodynamic functions.

For $\frac{h}{J} \gtrsim 0.52$, the percent difference (22) of the specific heat per site at $J|\beta = 500$ is $|PD(C)_{Fe}^{AF}| \lesssim 10^{-8}\%$.

Keeping $\frac{D}{J} = 0.51$ and increasing the temperature up to $J|\beta = 100$, we plot in Fig. 8a the specific heat per site versus $\frac{h}{J}$ of the ferromagnetic BEG model with $\frac{K}{J} = -2$ and the spin-1 AF Ising model in the interval $\frac{h}{J} \in [0.4, 0.6]$, showing that the two curves do not coincide in this whole interval. For $\frac{h}{J} \gtrsim 0.8$ we have $|PD(C)_{Fe}^{AF}| \lesssim 10^{-12}\%$, and at $\frac{h}{J} = 1.51$, when we have the transition of phases $B \rightleftharpoons E/E'$ in diagrams 6 at $T=0$, we obtain $PD(C)_{Fe}^{AF}\left(\frac{h}{J} = 1.51, \frac{D}{J} = 0.51; J|\beta = 100\right) \approx 4.59 \times 10^{-43}\%$.

For $\frac{D}{J} = 1$ we obtain in the whole interval of $\frac{h}{J}$, that is, $\frac{h}{J} \in [0, \infty)$,

$$|PD(C)_{Fe}^{AF}\left(\frac{h}{J}, \frac{D}{J} = 1; J|\beta = 500\right)| \lesssim 10^{-216}\%, \quad (24a)$$

$$|PD(C)_{Fe}^{AF}\left(\frac{h}{J}, \frac{D}{J} = 1; J|\beta = 100\right)| \lesssim 10^{-42}\%. \quad (24b)$$

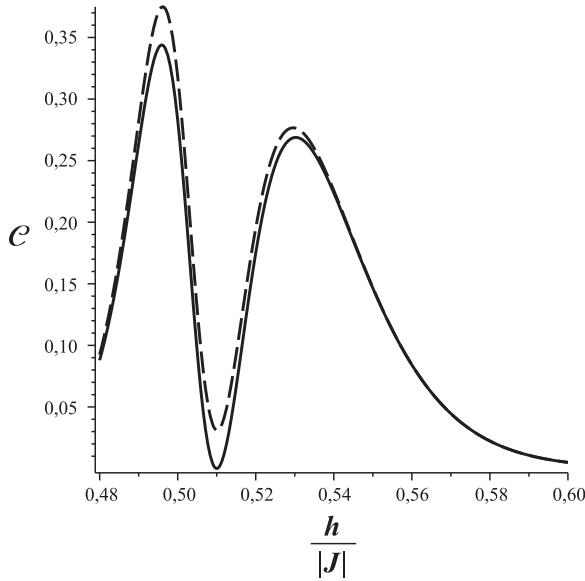


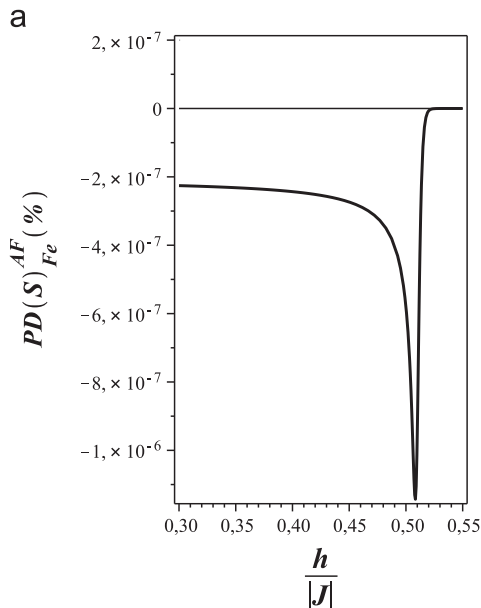
Fig. 8. The specific heat functions C per site of the ferromagnetic BEG model with $\frac{K}{J} = -2$ (solid line), and the spin-1 AF Ising model, with single-ion anisotropy term (dashed line), at $|J|\beta = 100$. Both curves are plotted for $\frac{D}{J} = 0.51$.

Fig. 9 shows the percent difference (22) for the entropy per site, $L = S$, with $\frac{D}{J} = 0.51$ at $|J|\beta = 500$. For these values of $\frac{D}{J}$ and $|J|\beta$, we obtain

$$PD(S)_{Fe}^{AF} \left(\frac{h}{|J|} = 0.8, \frac{D}{J} = 0.51; |J|\beta = 500 \right) \approx -4.68 \times 10^{-70}\%, \quad (25a)$$

$$|PD(S)_{Fe}^{AF} \left(\frac{h}{|J|} \geq 1.51, \frac{D}{J} = 0.51; |J|\beta = 500 \right)| \lesssim 10^{-439}\%. \quad (25b)$$

The curve $PD(S)_{Fe}^{AF} \times \frac{h}{|J|}$, at $|J|\beta = 100$ is plotted in **Fig. 9b** in the interval $\frac{h}{|J|} \in [0, 0.6]$. The value of the entropy per site for both models, for some values of $\frac{h}{|J|}$ in the same figure, that is



$$S_{Fe}^{BEG} \left(-1, \frac{h}{|J|} = 0, \frac{D}{J} = 0.51, \frac{K}{J} = -2; |J|\beta = 100 \right) \approx 1.037 \times 10^{-42}, \quad (26a)$$

$$S_{AF}^{Ising} \left(1, \frac{h}{|J|} = 0, \frac{D}{J} = 0.51, \frac{K}{J} = 0; |J|\beta = 100 \right) \approx 1.203 \times 10^{-42}, \quad (26b)$$

and

$$S_{Fe}^{BEG} \left(-1, \frac{h}{|J|} = 0.488, \frac{D}{J} = 0.51, \frac{K}{J} = -2; |J|\beta = 100 \right) \approx 6.417 \times 10^{-2}, \quad (26c)$$

$$S_{AF}^{Ising} \left(1, \frac{h}{|J|} = 0.488, \frac{D}{J} = 0.51, \frac{K}{J} = 0; |J|\beta = 100 \right) \approx 6.615 \times 10^{-2}. \quad (26d)$$

We also obtain that $|PD(S)_{Fe}^{AF}(\frac{h}{|J|} \sim 0.7, \frac{D}{J} = 0.51; |J|\beta = 500)| \lesssim 10^{-8}$ and $|PD(S)_{Fe}^{AF}(\frac{h}{|J|} \gtrsim 1.51, \frac{D}{J} = 0.51; |J|\beta = 100)| \lesssim 10^{-85}$.

Finally, for $\frac{D}{J} = 1$, the percent difference (22) of the entropy per site of the ferromagnetic BEG model, with $\frac{K}{J} = -2$, and the spin-1 AF Ising model is such that $|PD(S)_{Fe}^{AF}(\frac{h}{|J|}, \frac{D}{J} = 1; |J|\beta = 500)| \lesssim 10^{-215}$, and $|PD(S)_{Fe}^{AF}(\frac{h}{|J|}, \frac{D}{J} = 1; |J|\beta = 100)| \lesssim 10^{-42}$. Both inequalities are valid for $\frac{h}{|J|} \geq 0$.

5. Conclusions

We obtain the exact expression of the Helmholtz free energy (HFE) of the Blume–Emery–Griffiths (BEG) model in the presence of an external longitudinal magnetic field, for arbitrary values of the parameters in the Hamiltonian (2), valid for $T > 0$. The addition of the term $-K(S_i^z)^2(S_{i+1}^z)^2$ to the Hamiltonian of the spin-1 Ising model with single-ion anisotropy term and external longitudinal magnetic field, enriches the phase diagram of the latter at $T=0$ [5].

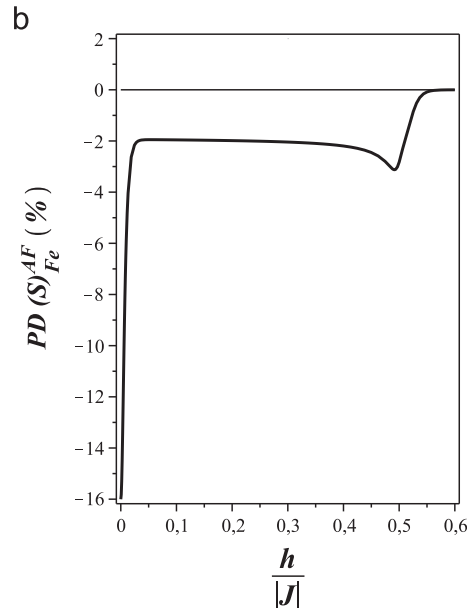


Fig. 9. The percent difference of the entropy per site between the ferromagnetic BEG model with $\frac{K}{J} = -2$, and the spin-1 AF Ising model, with single-ion anisotropy term, with $\frac{D}{J} = 0.51$. In (a), the curve is plotted at $|J|\beta = 500$; in (b), at $|J|\beta = 100$.

Although our results are valid for the ferromagnetic ($J < 0$) and AF ($J > 0$) versions of the BEG model, in the present paper we restrict our discussion to the results of the ferromagnetic BEG model and take $J = -1$. From Section 3 on, the parameters of the Hamiltonian (2) are scaled in units of $|J|$ and the inverse of temperature is measured as $|J|\beta$.

The thermodynamics of the ferromagnetic BEG model and of its respective phase diagram at $T=0$, is analyzed for two different regimes of the $\frac{K}{|J|}$ -parameter: $\frac{K}{|J|} < -1$ and $\frac{K}{|J|} \geq -1$. In both cases, the value of the z-component of the magnetization, M_z , at low temperature, is determined by the ground states of the model presented in Fig. 1. The function $M_z(\frac{h}{|J|})$ exhibits well-defined plateaux up to $|J|\beta \sim 1$ for $\frac{K}{|J|} \geq -1$; however, for $\frac{K}{|J|} \lesssim -1$ these plateaux are lost for $|J|\beta \gtrsim 10$.

The type of degeneracy of the ground state (exponential or non-exponential) along the lines that separate the phases in the phase diagram of the ferromagnetic BEG model, at $T=0$, determines the behavior of the entropy and specific heat, both per site, of the ferromagnetic model at low temperature. We show that for $\frac{K}{|J|} \geq -1$ the degeneracy of the ground state along the lines that separate the phases in Fig. 1b, at $T=0$, does not diverge in the thermodynamic limit ($N \rightarrow \infty$). In this region of values of $\frac{K}{|J|}$, the specific heat and the entropy, both per site, vanishes as $T \rightarrow 0$ in the presence of any external longitudinal magnetic field.

The lines that separate the phases in the diagram of Fig. 1a, where we have $\frac{K}{|J|} < -1$ and $T=0$, are related to ground states with exponential degeneracy. We calculated the degeneracy of the ground state along each of these lines and obtained their entropy per site at $T=0$, and then compared these results with the ones derived from the HFE of the ferromagnetic BEG at very low temperature. We have a strong indication that the results agree in the limit of $T \rightarrow 0$.

Finally for $\frac{K}{|J|} = -2$, the phase diagram of the ferromagnetic BEG model (see Fig. 6b), at $T=0$, with $\frac{D}{|J|} > \frac{1}{2}$ is identical to the phase diagram of the spin-1 AF Ising model, with single-ion anisotropy term, at $T=0$ (see Fig. 6a).

We compared the thermodynamics of both models at very low temperature ($|J|\beta \sim 500$), when the largest contribution to their thermodynamic is expected to come from their respective ground states. At temperature $|J|\beta = 500$, the function $M_z(\frac{h}{|J|})$ of both models coincide by at least 1 part in 10^{14} . Such agreement decreases as the temperature increases.

The ferromagnetic and AF nature of the models is not apparent when we measure M_z in the interval of $\frac{h}{|J|} \in [0, \infty)$. They are distinguished, however, by the specific heat per site and the entropy per site for $\frac{D}{|J|} \sim 0.51$, when $2D \sim |J|$, and for values of the external magnetic field such that $2h \sim |J|$, even at low temperatures, $|J|\beta = 500$. At this temperature and with this value of the parameter $\frac{D}{|J|}$, the specific heat per site under $\frac{h}{|J|} = 0.51$ are valued $C_{Fe}^{BEG} \sim 10^{-213}$ and $C_{AF}^{Ising} \sim 10^{-8}$ for the BEG and Ising models, respectively: their values differ by 205 orders of magnitude. We cannot explain this difference. When the value of the parameter $\frac{D}{|J|}$ is such that $2D \gg |J|$, the specific heat per site and the entropy per site are insensitive, at low temperature, if the model is ferromagnetic ($J = -1$) or AF ($J=1$).

The information about the exact thermodynamics of the staggered BEG model in the presence of an external longitudinal magnetic field can be obtained from the thermodynamics of the BEG model through the relation (4). The study of the AF BEG model is currently under way. We expect to present our results in the near future.

Acknowledgements

M.T. Thomaz thanks Professor J.F. Stilck for interesting discussions about the degeneracy in the phase diagram of the BEG model.

Appendix A. The exact HFE of the $D=1$ BEG model in the presence of a longitudinal magnetic field

The transfer matrix method [2–4] was used by Krinsky and Furman [10] to calculate the HFE of the BEG model in the presence of a longitudinal magnetic field ($L=0$ in Hamiltonian (1.1) of Ref. [10]).

In this appendix we follow the steps of Ref. [5], but here we write the root of cubic equation (A.4) with the largest modulus as a real number, obtaining the exact HFE of the model (2).

The partition function $\mathcal{Z}(J, h, D; \beta)$ of the BEG Hamiltonian (2) is equal to [4]

$$\mathcal{Z}(J, h, D, K; \beta) = \text{Tr}[\mathbf{U}^N], \quad (\text{A.1})$$

where N is the number of sites in the periodic chain and the matrix \mathbf{U} for the symmetric Hamiltonian (2) is

$$\mathbf{U}(J, h, D, K; \beta) = \begin{bmatrix} e^{-\beta(J+2h+2D-K)} & e^{-\beta(h+D)} & e^{-\beta(-J+2D-K)} \\ e^{-\beta(h+D)} & 1 & e^{-\beta(-h+D)} \\ e^{-\beta(-J+2D-K)} & e^{-\beta(-h+D)} & e^{-\beta(J-2h+2D-K)} \end{bmatrix}, \quad (\text{A.2})$$

and $\beta = \frac{1}{kT}$, in which k is the Boltzmann's constant and T is the absolute temperature in kelvin.

The matrix $\mathbf{U}(J, h, D, K; \beta)$ is hermitian for any value of J, h, D, K and β . Its three eigenvalues are real. The matrices \mathbf{U} [see Eq. (A.2)] and \mathbf{T} [in Ref. [10]] differ by a rearrangement of lines and the sign of the external magnetic field h . The partition function (A.1) is an even function of h .

In the thermodynamic limit ($N \rightarrow \infty$), the partition function (A.1) of the model and its HFE \mathcal{W} are, respectively,

$$\begin{aligned} \mathcal{Z}(J, h, D, K; \beta) &= (\lambda_1)^N \quad \text{and} \quad \mathcal{W}(J, h, D, K; \beta) \\ &= -\frac{1}{\beta} \ln[\lambda_1(J, h, D; \beta)], \end{aligned} \quad (\text{A.3})$$

for non-degenerate eigenvalues of \mathbf{U} . We assume that λ_1 is the eigenvalue of matrix \mathbf{U} with the largest modulus, root of the cubic equation

$$-\lambda^3 + P\lambda^2 + Q\lambda + R = 0, \quad (\text{A.4})$$

in which

$$P = 1 + 2e^{-\beta(J+2D-K)} \cosh(2\beta h) = \text{Tr}[\mathbf{U}] \quad (\text{A.5a})$$

$$\begin{aligned} Q &= 4e^{-2\beta D} e^{-\frac{\beta(J-K)}{2}} \cosh(2\beta h) \sinh\left(\frac{\beta(J-K)}{2}\right) \\ &\quad + 2e^{-2\beta(2D-K)} \sinh(2\beta J), \end{aligned} \quad (\text{A.5b})$$

$$R = -2e^{-2\beta(2D-K)} \sinh(2\beta J) + 4e^{-\beta(4D-K)} \sinh(\beta J). \quad (\text{A.5c})$$

The uniqueness of this eigenvalue for the matrix (A.2) is ensured by the Perron–Frobenius Theorem [11] for any temperature T .

The roots of the cubic equation (A.4) are well known [12]. The root with the largest modulus is

$$\lambda_1 = 2\sqrt{-Q} \cos\left(\frac{\theta}{3}\right) + \frac{P}{3} \quad (\text{A.6})$$

where

$$\cos(\theta) = \frac{\bar{R}}{\sqrt{(-\bar{Q})^3}} \quad (\text{A.7a})$$

with

$$\bar{Q} = -\frac{3Q + P^2}{9} \quad \text{and} \quad \bar{R} = \frac{9QP + 27R + 2P^3}{54}. \quad (\text{A.7b})$$

The expression of λ_1 has cubic roots. Plotting the thermodynamic functions of the BEG model required numerical evaluation of that expression. In this work the CAS `Maple` has been used, and some spurious complex values (probably due to the way the cubic roots are handled by the system) appeared in the floating point evaluation even for 700 significant digits, so some caution had to be taken. The expression (A.3) of the HFE, valid at any temperature T and obtained from Eqs. (A.6)–(A.7b), is exact for the ferromagnetic ($J < 0$) and the AF ($J > 0$) BEG models in the presence of a longitudinal external magnetic field.

Appendix B. The states and energies of the dimers

For spin-1 there are nine possible dimers in neighbouring sites of the chain. Those states and their corresponding energies, obtainable from Eq. (6) are

$$|D^{(A)}\rangle_{i,i+1} \equiv |0\rangle_i \otimes |0\rangle_{i+1} \quad \text{and} \quad \frac{\varepsilon_{i,i+1}^{(A)}}{|J|} = 0, \quad (\text{B.1})$$

$$|D^{(B)}\rangle_{i,i+1} \equiv |1\rangle_i \otimes |1\rangle_{i+1} \quad \text{and} \quad \frac{\varepsilon_{i,i+1}^{(B)}}{|J|} = -1 + \frac{2D}{|J|} - \frac{2h}{|J|} - \frac{K}{|J|}, \quad (\text{B.2})$$

$$|D^{(C)}\rangle_{i,i+1} \equiv |-1\rangle_i \otimes |-1\rangle_{i+1} \quad \text{and} \quad \frac{\varepsilon_{i,i+1}^{(C)}}{|J|} = -1 + \frac{2D}{|J|} + \frac{2h}{|J|} - \frac{K}{|J|}, \quad (\text{B.3})$$

$$|D^{(E_1)}\rangle_{i,i+1} \equiv |0\rangle_i \otimes |1\rangle_{i+1} \quad \text{and} \quad \frac{\varepsilon_{i,i+1}^{(E_1)}}{|J|} = \frac{D}{|J|} - \frac{h}{|J|}, \quad (\text{B.4a})$$

$$|D^{(E_2)}\rangle_{i,i+1} \equiv |1\rangle_i \otimes |0\rangle_{i+1} \quad \text{and} \quad \frac{\varepsilon_{i,i+1}^{(E_2)}}{|J|} = \frac{D}{|J|} - \frac{h}{|J|}, \quad (\text{B.4b})$$

$$|D^{(F_1)}\rangle_{i,i+1} \equiv |0\rangle_i \otimes |-1\rangle_{i+1} \quad \text{and} \quad \frac{\varepsilon_{i,i+1}^{(F_1)}}{|J|} = \frac{D}{|J|} + \frac{h}{|J|}, \quad (\text{B.5a})$$

$$|D^{(F_2)}\rangle_{i,i+1} \equiv |-1\rangle_i \otimes |0\rangle_{i+1} \quad \text{and} \quad \frac{\varepsilon_{i,i+1}^{(F_2)}}{|J|} = \frac{D}{|J|} + \frac{h}{|J|}, \quad (\text{B.5b})$$

$$|D^{(G_1)}\rangle_{i,i+1} \equiv |1\rangle_i \otimes |-1\rangle_{i+1} \quad \text{and} \quad \frac{\varepsilon_{i,i+1}^{(G_1)}}{|J|} = 1 + \frac{2D}{|J|} - \frac{K}{|J|}, \quad (\text{B.6a})$$

$$|D^{(G_2)}\rangle_{i,i+1} \equiv |-1\rangle_i \otimes |1\rangle_{i+1} \quad \text{and} \quad \frac{\varepsilon_{i,i+1}^{(G_2)}}{|J|} = 1 + \frac{2D}{|J|} - \frac{K}{|J|}. \quad (\text{B.6b})$$

Appendix C. The ground states and energies of the BEG model in the presence of a longitudinal magnetic field

We assume that the chain has a even number of sites N by letting $N = 2M$, in which M is a positive integer. In the thermodynamic limit ($N \rightarrow \infty$), we also have $M \rightarrow \infty$. The ground state vectors at each phase in the phase diagram in Fig. 1b at $T=0$ are

$$|\Psi_0\rangle_A = |0\rangle_1 \otimes |0\rangle_2 \otimes \cdots \otimes |0\rangle_{2M}, \quad (\text{C.1a})$$

$$|\Psi_0\rangle_B = |1\rangle_1 \otimes |1\rangle_2 \otimes \cdots \otimes |1\rangle_{2M}, \quad (\text{C.1b})$$

$$|\Psi_0\rangle_C = |-1\rangle_1 \otimes |-1\rangle_2 \otimes \cdots \otimes |-1\rangle_{2M}, \quad (\text{C.1c})$$

$$|\Psi_0\rangle_E = |0\rangle_1 \otimes |1\rangle_2 \otimes |0\rangle_3 \otimes |1\rangle_4 \otimes \cdots \otimes |0\rangle_{2M-1} \otimes |1\rangle_{2M}, \quad (\text{C.1d})$$

$$|\Psi_0\rangle_{E'} = |1\rangle_1 \otimes |0\rangle_2 \otimes |1\rangle_3 \otimes |0\rangle_4 \otimes \cdots \otimes |1\rangle_{2M-1} \otimes |0\rangle_{2M}, \quad (\text{C.1e})$$

$$|\Psi_0\rangle_F = |0\rangle_1 \otimes |-1\rangle_2 \otimes |0\rangle_3 \otimes |-1\rangle_4 \otimes \cdots \otimes |0\rangle_{2M-1} \otimes |-1\rangle_{2M}, \quad (\text{C.1f})$$

$$|\Psi_0\rangle_{F'} = |-1\rangle_1 \otimes |0\rangle_2 \otimes |-1\rangle_3 \otimes |0\rangle_4 \otimes \cdots \otimes |-1\rangle_{2M-1} \otimes |0\rangle_{2M}. \quad (\text{C.1g})$$

One is reminded that $S_i^z |s\rangle_i = s |s\rangle_i$, $s \in \{0, \pm 1\}$ and $i \in \{1, 2, \dots, 2M\}$.

The states $|\Psi_0\rangle_{E'}$, $|\Psi_0\rangle_{F'}$ and $|\Psi_0\rangle_{G'}$ have the same energies as the states $|\Psi_0\rangle_E$, $|\Psi_0\rangle_F$ and $|\Psi_0\rangle_G$, respectively.

The values of the ground state energy of the phases A, B, E(E') and F(F') for $\frac{h}{|J|} \geq 0$, are, respectively,

$$\frac{E_0^A}{|J|} = 0, \quad (\text{C.2a})$$

$$\frac{E_0^B}{|J|} = 2M \left(\frac{J}{|J|} + \frac{2D}{|J|} - \frac{2h}{|J|} - \frac{K}{|J|} \right), \quad (\text{C.2b})$$

$$\frac{E_0^E}{|J|} = 2M \left(\frac{D}{|J|} - \frac{h}{|J|} \right) = \frac{E_0^{E'}}{|J|}, \quad (\text{C.2c})$$

$$\frac{E_0^F}{|J|} = 2M \left(\frac{D}{|J|} + \frac{h}{|J|} \right) = \frac{E_0^{F'}}{|J|}. \quad (\text{C.2d})$$

The phase diagram of the AF spin-1 Ising model, with a single-ion anisotropy term, in the presence of an external longitudinal magnetic field has an extra phase [5] at $T=0$, the Néel state, given by the vector states

$$|\Psi_0\rangle_G = |1\rangle_1 \otimes |-1\rangle_2 \otimes |1\rangle_3 \otimes |-1\rangle_4 \otimes \cdots \otimes |1\rangle_{2M-1} \otimes |-1\rangle_{2M}, \quad (\text{C.3a})$$

$$|\Psi_0\rangle_{G'} = |-1\rangle_1 \otimes |1\rangle_2 \otimes |-1\rangle_3 \otimes |1\rangle_4 \otimes \cdots \otimes |-1\rangle_{2M-1} \otimes |1\rangle_{2M}. \quad (\text{C.3b})$$

The ground state energy, in units of $|J|$, of these states G and G' is

$$\frac{E_0^G}{|J|} = \frac{E_0^{G'}}{|J|} = 2M \left(-\frac{J}{|J|} + \frac{2D}{|J|} - \frac{K}{|J|} \right) = \frac{E_0^{G'}}{|J|}. \quad (\text{C.4})$$

Appendix D. Degeneracy of ground states along transition lines and on critical points of phase diagrams of the ferromagnetic BEG model with $\frac{K}{J} < -1$ at $T=0$

Let us take the transition $A \rightleftharpoons E/E'$ as an example for the calculation of the degeneracy of the ground states along the boundary of two phases in the phase diagram in Fig. 1a of the ferromagnetic BEG model at $T=0$. The critical point \mathcal{T} , excluded from this analysis, will be treated subsequently. For all points in the vicinity of (but not upon) this line, the chain may be found in either one of the following states, among those listed in Appendix C:

$$|\Psi_0\rangle_A = |0\rangle_1 \otimes |0\rangle_2 \otimes \cdots \otimes |0\rangle_{2M}, \quad (\text{D.1})$$

$$|\Psi_0\rangle_E = |0\rangle_1 \otimes |1\rangle_2 \otimes |0\rangle_3 \otimes |1\rangle_4 \otimes \cdots \otimes |0\rangle_{2M-1} \otimes |1\rangle_{2M}, \quad (\text{D.2})$$

$$|\Psi_0\rangle_{E'} = |1\rangle_1 \otimes |0\rangle_2 \otimes |1\rangle_3 \otimes |0\rangle_4 \otimes \cdots \otimes |1\rangle_{2M-1} \otimes |0\rangle_{2M}. \quad (\text{D.3})$$

Hence, on the phase transition line, if the i -th site (for $i \in \{1, 2, \dots, 2M-1\}$, in which M is an integer) happens to be in the state $|0\rangle_i$, the state of the $(i+1)$ -th site may be either $|0\rangle_{i+1}$ or $|1\rangle_{i+1}$. On the other hand, if the i -th site state is $|1\rangle_i$, the state of the $(i+1)$ -th site must be $|0\rangle_{i+1}$. In other words, the energy constraint on this phase transition line imposes some *sequencing rules* on the states of the chain: each $|0\rangle_{i+1}$ succeeds either a $|0\rangle_i$ or a $|1\rangle_i$; and each $|1\rangle_{i+1}$ succeeds a $|0\rangle_i$. (Equivalently: $|1\rangle_{i+1}$ never succeeds $|1\rangle_i$.)

Let $g_{|0\rangle}^{(i)}$ and $g_{|1\rangle}^{(i)}$ be the number of possible occurrences of the one-site states $|0\rangle$ and $|1\rangle$ at the i -th site, respectively. The number of possible occurrences for each state at the $(i+1)$ -th site can thus be written as a recurrence relation of the form

$$g^{(i+1)} = T g^{(i)}, \quad (\text{D.4})$$

in which

$$g^{(i)} = \begin{bmatrix} g_{|0\rangle}^{(i)} \\ g_{|1\rangle}^{(i)} \end{bmatrix}, \quad g^{(1)} = \begin{bmatrix} 1 \\ 1 \end{bmatrix}, \quad \text{and} \quad T = \begin{bmatrix} 1 & 1 \\ 1 & 0 \end{bmatrix}. \quad (\text{D.5})$$

The configuration $g^{(1)}$ corresponds to the chain with one site ($i=1$), in which we may have either the state $|0\rangle_1$ or the state $|1\rangle_1$.

Such recurrence generalizes to

$$g^{(i+p)} = T^p g^{(i)}, \quad (\text{D.6})$$

and hence we may write, relating the 1-st and $(2M)$ -th (last) sites,

$$g^{(2M)} = T^{2M-1} g^{(1)}. \quad (\text{D.7})$$

The total number of states with the same ground state energy corresponds to the sum of all possibilities for the $|0\rangle$ and $|1\rangle$ states at the $(2M)$ -th state. It is then equivalent to the L^1 -norm of the vector $g^{(2M)}$,

$$\Omega_{A \rightleftharpoons E/E'} = |g^{(2M)}|_1 = g_{|0\rangle}^{(2M)} + g_{|1\rangle}^{(2M)}; \quad (\text{D.8})$$

hence, we should turn our attention to the evaluation of the matrix power T^{2M-1} in (D.7). The matrix T can be easily diagonalized, yielding

$$\Lambda_{A \rightleftharpoons E/E'} = \begin{bmatrix} \frac{1}{2}(1 + \sqrt{5}) & 0 \\ 0 & \frac{1}{2}(1 - \sqrt{5}) \end{bmatrix} \quad (\text{D.9})$$

and the corresponding matrix of eigenvectors,

$$\mathbf{D}_{A \rightleftharpoons E/E'} = \begin{bmatrix} \frac{2}{1 + \sqrt{5}} & \frac{2}{1 - \sqrt{5}} \\ 1 & 1 \end{bmatrix}, \quad (\text{D.10a})$$

so that

$$\mathbf{D}_{A \rightleftharpoons E/E'}^{-1} T \mathbf{D}_{A \rightleftharpoons E/E'} = \Lambda_{A \rightleftharpoons E/E'}. \quad (\text{D.10b})$$

We rewrite (D.7) as

$$g^{(2M)} = \mathbf{D}_{A \rightleftharpoons E/E'}^{-1} \Lambda_{A \rightleftharpoons E/E'}^{N-1} \mathbf{D}_{A \rightleftharpoons E/E'} g^{(1)}. \quad (\text{D.11})$$

After some algebra, (D.8) yields the degeneracy of the ground states along the transition line $A \rightleftharpoons E/E'$ in Fig. 1a, at $T=0$,

$$\Omega_{A \rightleftharpoons E/E'} = \frac{1}{2^{2M}} \left[\frac{5 + 3\sqrt{5}}{10} (1 + \sqrt{5})^{2M} + \frac{5 - 3\sqrt{5}}{10} (1 - \sqrt{5})^{2M} \right]. \quad (\text{D.12})$$

Thus the corresponding entropy for this transition is

$$S_{A \rightleftharpoons E/E'} = \lim_{M \rightarrow \infty} \frac{\ln \Omega_{A \rightleftharpoons E/E'}}{2M} = \ln \left(\frac{1 + \sqrt{5}}{2} \right) = \ln \varphi, \quad (\text{D.13a})$$

$$\approx 0.48121, \quad (\text{D.13b})$$

in which φ is the celebrated golden ratio.

The reader should notice that the periodic spatial boundary condition on the chain (cf. Section 1) *has not been used at all* in the calculation of the degeneracy (D.12) and hence on the determination of the entropy per site (D.13b). We shall describe in what follows how the degeneracy can be calculated taking that condition into account; the value of the entropy per site (D.13b), however, will not change. By identifying the $(N+1)$ -th site of the chain with its 1-st site, the sequencing rules described in the beginning of this appendix should also apply to the N -th and 1-st site. Here we have $N = 2M$. Namely, if the chain has $|1\rangle_1$ in its 1-st site, it cannot have $|1\rangle_{2M}$ in its $2M$ -th site. On the other hand, if the chain begins with $|0\rangle_1$, there are no restrictions: it can end in either $|0\rangle_{2M}$ or $|1\rangle_{2M}$. The two branches of possibilities — chain starting with $|0\rangle_1$ or chain starting with $|1\rangle_1$ — can be described separately by the 1-st site conditions

$$g^{(1),0} = \begin{bmatrix} 1 \\ 0 \end{bmatrix}, \quad g^{(1),1} = \begin{bmatrix} 0 \\ 1 \end{bmatrix}. \quad (\text{D.14})$$

The version of (D.7) upon boundary conditions reads

$$g_{B.C.}^{(2M)} = R_0 T^{2M-1} g^{(1),0} + R_1 T^{2M-1} g^{(1),1}, \quad (\text{D.15})$$

in which $\{R_0, R_1\}$ are matrices that implement the pertinent restrictions to each 1-st site condition. In the present situation, these matrices have the form

$$R_0 = \begin{bmatrix} 1 & 0 \\ 0 & 1 \end{bmatrix} \quad \text{and} \quad R_1 = \begin{bmatrix} 1 & 0 \\ 0 & 0 \end{bmatrix}. \quad (\text{D.16})$$

The first term in (D.15) relates to the chain states with a $|0\rangle_1$ state; R_0 is simply the identity matrix, and there are no restrictions to the which state the $2M$ -th site may have. On the other hand, the second term in (D.15) relates to the chain states with a $|1\rangle_1$ state; the effect of R_1 on $T^{2M-1} g^{(1),1}$ is that of discarding all possible chain states with a $|1\rangle_{2M}$ state, which would violate the energy condition/sequencing rules. (Notice that, without boundary conditions, we would have R_0 and R_1 both equal to the identity matrix, and (D.15) would be reduced to (D.7). The 1-st site condition Eq. (D.5) is equivalent to letting $g^{(1)} = g^{(1),0} + g^{(1),1}$.) The total number of states with the same ground state energy corresponds to

$$\Omega_{A \rightleftharpoons E/E'}^{B.C.} = |g_{B.C.}^{(2M)}|_1 = g_{B.C.,|0\rangle}^{(2M)} + g_{B.C.,|1\rangle}^{(2M)}, \quad (\text{D.17})$$

analogous to (D.8); here, $g_{B.C.,|0\rangle}^{(2M)}$ and $g_{B.C.,|1\rangle}^{(2M)}$ are the components of $g_{B.C.}^{(2M)}$. We obtain

$$\Omega_{A \rightleftharpoons E/E'}^{B.C.} = \frac{1}{2^M} \left[(1 + \sqrt{5})^{2M} + (1 - \sqrt{5})^{2M} \right], \quad (D.18)$$

which differs from the degeneracy (D.12); however, the same entropy per site is obtained from (D.18) as it is obtained from (D.12),

$$S_{A \rightleftharpoons E/E'}^{B.C.} = \lim_{M \rightarrow \infty} \frac{\ln \Omega_{A \rightleftharpoons E/E'}^{B.C.}}{2M} = S_{A \rightleftharpoons E/E'}, \quad (D.19)$$

given by (D.13a).

The analysis for the critical point \mathcal{T} is analogous. In the vicinity of (but not on) \mathcal{T} , the available states are

$$|\Psi_0\rangle_A = |0\rangle_1 \otimes |0\rangle_2 \otimes \cdots \otimes |0\rangle_{2M}, \quad (D.20a)$$

$$|\Psi_0\rangle_E = |0\rangle_1 \otimes |1\rangle_2 \otimes |0\rangle_3 \otimes |1\rangle_4 \otimes \cdots \otimes |0\rangle_{2M-1} \otimes |1\rangle_{2M}, \quad (D.20b)$$

$$|\Psi_0\rangle_{E'} = |1\rangle_1 \otimes |0\rangle_2 \otimes |1\rangle_3 \otimes |0\rangle_4 \otimes \cdots \otimes |1\rangle_{2M-1} \otimes |0\rangle_{2M}, \quad (D.20c)$$

$$|\Psi_0\rangle_F = |0\rangle_1 \otimes | - 1\rangle_2 \otimes |0\rangle_3 \otimes | - 1\rangle_4 \otimes \cdots \otimes | - 1\rangle_{2M}, \quad (D.20d)$$

$$|\Psi_0\rangle_{F'} = | - 1\rangle_1 \otimes |0\rangle_2 \otimes | - 1\rangle_3 \otimes |0\rangle_4 \otimes \cdots \otimes | - 1\rangle_{2M-1} \otimes |0\rangle_{2M}. \quad (D.20e)$$

Hence, for the state \mathcal{T} , the i -th site may be in any one of the states $\{| - 1\rangle_i, |0\rangle_i, |1\rangle_i\}$, $i \in \{1, 2, \dots, 2M\}$. Moreover, for $i \in \{1, 2, \dots, 2M - 1\}$, the state $| - 1\rangle_{i+1}$ can only be preceded by $|0\rangle_i$, the state $|0\rangle_{i+1}$ can be preceded by $| - 1\rangle_i$ or $|0\rangle_i$ or $|1\rangle_i$, and the state $|1\rangle_{i+1}$ can only be preceded by $|0\rangle_i$ in order to guarantee that the dimer has the least possible value of energy. (Equivalently: $| - 1\rangle_{i+1}$ never succeeds either $| - 1\rangle_i$ or $|1\rangle_i$; $|1\rangle_{i+1}$ never succeeds either $| - 1\rangle_i$ or $|1\rangle_i$.) The recurrence relation among the number of possibilities for each state at a site can be expressed as a recurrence relation of the same form as (D.7), but now with

$$g^{(i)} = \begin{bmatrix} g_{|-1\rangle}^{(i)} \\ g_{|0\rangle}^{(i)} \\ g_{|1\rangle}^{(i)} \end{bmatrix}, \quad g^{(1)} = \begin{bmatrix} 1 \\ 1 \\ 1 \end{bmatrix}, \quad \text{and} \quad T = \begin{bmatrix} 0 & 1 & 0 \\ 1 & 1 & 1 \\ 0 & 1 & 0 \end{bmatrix}. \quad (D.21)$$

The diagonalization of T leads us to

$$A_{\mathcal{T}} = \begin{bmatrix} 2 & 0 & 0 \\ 0 & -1 & 0 \\ 0 & 0 & 0 \end{bmatrix} \quad (D.22a)$$

and

$$D_{\mathcal{T}} = \begin{bmatrix} 1 & 1 & -1 \\ 2 & -1 & 0 \\ 1 & 1 & 1 \end{bmatrix}. \quad (D.22b)$$

By calculating $g^{(2M)}$ as in the previous situation, [see Eq. (D.12)], we obtain the degeneracy at the critical point \mathcal{T} in Fig. 1a,

$$\Omega_{\mathcal{T}} = \frac{1}{3} \left(2^{2M+2} - 1 \right), \quad (D.23)$$

and the corresponding entropy

$$S_{\mathcal{T}} = \lim_{M \rightarrow \infty} \frac{\ln \Omega_{\mathcal{T}}}{2M} = \ln(2), \quad (D.24a)$$

$$\approx 0.69315. \quad (D.24b)$$

Once again, the calculation of the degeneracy under the boundary conditions may be carried out in the same fashion as for the $A \rightleftharpoons E/E'$ transition. Even though the degeneracy itself differs from that of the unconditioned case,

$$\Omega_{\mathcal{T}}^{B.C.} = 2^{2M} + 1, \quad (D.25)$$

the entropy per site obtained is the same,

$$S_{\mathcal{T}}^{B.C.} = \lim_{M \rightarrow \infty} \frac{\ln \Omega_{\mathcal{T}}^{B.C.}}{2M} = S_{\mathcal{T}}. \quad (D.26)$$

The degeneracies and entropies for the other phase transition lines in the phase diagram of the ferromagnetic BEG model with $\frac{K}{J|l|} < -1$, at $T=0$, and the critical point \mathcal{R} can be obtained in the same fashion.

It is important to point out that in order to calculate the entropy per site of the ferromagnetic BEG model along phase boundaries and multicritical points at $T=0$ we can calculate the total number of degenerate ground states in the chain without taking into account the periodic spatial boundary condition.

References

- [1] J. Simon, et al., *Nature* 472 (04/21/2011) 307 (and references therein).
- [2] H.A. Kramers, G.H. Wannier, *Phys. Rev.* 60 (1941) 252.
- [3] H.A. Kramers, G.H. Wannier, *Phys. Rev.* 60 (1941) 263.
- [4] R.J. Baxter, *Exactly Solved Models in Statistical Mechanics*, Academic Press, London, 1989 (Section 2.1).
- [5] S.M. de Souza, M.T. Thomaz, *J. Magn. Magn. Mater.* 354 (2014) 205.
- [6] M. Blume, V.J. Emery, R.B. Griffiths, *Phys. Rev. A* 4 (1971) 1071.
- [7] M. Blume, *Phys. Rev.* 141 (1966) 517.
- [8] H.W. Capel, *Physica (Utrecht)* 32 (1966) 966; H.W. Capel, *Physica (Utrecht)* 33 (1967) 295.
- [9] J. Bernasconi, F. Rys, *Phys. Rev. B* 9 (1971) 3045.
- [10] S. Krinsky, D. Furman, *Phys. Rev. B* 11 (1975) 2602.
- [11] B. Simon, *The Statistical Mechanics of Lattice Gases*, vol. 1, Princeton University Press, Princeton, NJ, 1993.
- [12] M.R. Spiegel, *Mathematical Handbook of Formula and Tables*, Schaum's Outline Series, Singapore, 1990, p. 32.
- [13] F. Reif, *Statistical Thermal Physics*, International Student Edition, Mc Graw-Hill Kogakusha Ltd., Tokyo, 1965, Section 3.3.